Modeling Microbial Growth and Biosynthesis of Medium Chain Length Polyhydroxyalkanoate (PHA) by *Pseudomonas putida* LS46

By

Shabnam Sharifyazd

A Thesis Submitted to the Faculty of Graduate Studies of

The University of Manitoba

In partial fulfillment of the requirements for the degree of

Master of Science

Department of Civil Engineering

University of Manitoba

Winnipeg

Abstract

In 2015, 322 million tonnes petroleum-based plastics were produced in the world. The detrimental effects of petro-plastics on the environment highlight the need for bio-based, biodegradable plastics. Among different types of thermoplastics, Polyhydroxyalkanoates (PHAs) with different physical/mechanical and thermal properties are well known, as they are biodegradable, biocompatible, and non-toxic. However, the main drawback of PHA biosynthesis in large scale is the high cost of production. It is known that PHA production can be considerably increased under oxygen-limited conditions. In this study, growth and synthesis of medium chain length PHAs (mcl-PHAs) by *Pseudomonas putida* LS46 cultured with octanoic acid under oxygen-limited conditions in the batch mode was modeled. Four models including the Monod model incorporated Leudeking–Piret (MLP), the Moser model incorporated Leudeking–Piret (Moser-LP), the Logistic model incorporated Leudeking–Piret (LLP), and the Modified Logistic model incorporated Leudeking–Piret (MLLP) were investigated. The experimental data related to 0%, 1%, 5%, 10%, and 40% dissolved oxygen (DO) were employed for the modeling. The data corresponding to 0%, 1% and 5% DO were used for calibration and validation of the model and the data related to 10% and 40% DO were used for investigating the validity of the model under oxygen excess conditions. Kinetic parameters of each model were calibrated by using the multi-objective optimization algorithm, Pareto Archived Dynamically Dimensioned Search (PA-DDS) by minimizing the sum of absolute error (SAE) for PHA production and growth simultaneously. Among the four models, MLP and Moser-LP models adequately represented the experimental data for oxygen limited conditions. In addition, the calibrated value of maximum specific growth rate for MLP and Moser-LP models (0.497 and 0.622) were within its experimental value (0.578 ± 0.142). In addition, the MLP and Moser-LP models could not adequately simulate PHA

production at 10% and 40% DO, confirming the fact that the models were not valid under oxygen excess conditions. For growth, under oxygen excess conditions, this deviation was not very significant.

Acknowledgements

In fact, no word can express my gratitude to my supervisors Dr. Masoud Asadzadeh and Dr. David Levin for their generous support throughout my master's program. Their friendly guidance, encouraging thoughts, and patience helped me step forward in my research. Dr. Asadzadeh and Dr. Levin are my role models and I am honored to work under their kind supervision.

I would like to thank my defence committee members, Dr. Hartmut Hollander and Dr. Stefan Cenkowski for their continued support and valuable suggestions throughout my studies.

I would like to take this opportunity to thank Warren Blunt for providing data for this thesis.

I also want to thank my family and friends for always being encouraging and patient with me, and supporting me in achieving my dreams.

Contents

List of Tables

List of Figures

Abbreviations

α, β	Constants in models Monod incorporated Leudeking–Piret, Logistic incorporated Leudeking–Piret, and Monod incorporated modified Leudeking–Piret
DO	Dissolved oxygen
FadG	R-specific ketoacyl-CoA reductase
K_b	Half-saturation coefficient (g L^{-1})
$K_{I,S}$	Substrate-inhibition constant (g L^{-1})
K_s	Substrate saturation constant (g L^{-1})
LCFAs	Long chain fatty acids
LLP	Logistic incorporated Leudeking–Piret
MLP	Monod incorporated Leudeking–Piret
MLLP	Monod incorporated modified Leudeking–Piret
MSE	Mean squared error
n	Fitting constant
NADPH	Nicotinamide adenine dinucleotide phosphate
NFE	Number of function evaluations (Computational budget)
p	Perturbation probability
P	Product concentration (g L^{-1})
P_0, P_t	Product concentration at initial and at anytime 't' (g L^{-1})
PF	Pareto optimal front
PHA	Polyhydroxyalkanoates
PhaC	PHA synthase enzyme
PhaJ	Trans-enoyl-CoA hydratase

PHB	Polyhydroxybutyrate
PHBV	Poly(3-hydroxybutyrate-*co*-3-hydroxyvalerate)
PS	Set of optimal solutions
q	Initial solution count
Q_v	Volumetric productivity (g PHA L^{-1} h^{-1})
r	Exponent in model Monod incorporated modified Leudeking–Piret (MLLP)
R^2	Coefficient of determination
S	Limiting substrate concentration (g L^{-1})
SAE	Sum of absolute error
SSE	Sum of squared error
t	Time (h)
X	Biomass concentration (g L^{-1})
x^{curr}	Current solution of PA-DDS algorithm
X_i	Measured data
X_0, X_m	Initial and maximum biomass concentration (g L^{-1})
x^{min}, x^{max}	Victors of decision variable boundaries
x^{new}	New solution in PA-DDS algorithm
X_{PHA}	PHA biomass (g L^{-1})
X_r	Residual cell mass (g L^{-1})
X_t	Biomass concentration at anytime 't' (g L^{-1})
X_T	Total biomass (g L^{-1})
$\widehat{X}_i$	Estimated data by model
μ, μ_{max}	Specific growth rate, maximum specific growth rate (h^{-1})

$\%_{PHA}$	Intracellular PHA content (% g g^{-1})

Chapter 1

Literature review

1. Introduction

1.1. Plastics and Bioplastics

Petroleum-based (petro-)plastics, with their extensive applications in different fields including transportation, clothes, food packing, construction, medical supplies, communication and leisure industries, have transformed our daily lives (Thompson et al. 2009; Iwata 2015). Widespread use of petro-plastics started from 1950s, and in 2015 global production of these materials had risen to 322 million tonnes. With current trends in production, it is predicted to reach 33 billion tonnes of plastics by 2050 (PlasticsEurope 2016, 2012; Worm et al. 2017; Rochman et al. 2013).

Petro-plastics are produced from petrochemical products. Approximately, 10% of the oil and gas that is produced and imported by the United States is applied in the plastic industry (DiGregorio 2009). Petro-plastics are highly recalcitrant to natural biodegradation processes and thus significant amounts of plastic wastes have accumulated in the environment. It is estimated that some petro-plastic wastes may remain in the environment for 2,000 years or longer (DiGregorio 2009). Petro-plastic wastes cause greenhouse gas emissions and ecological damage specifically in the oceans where options for removal are extremely limited (Hopewell et al. 2009; Jambeck et al. 2015; Worm et al. 2017). In addition, there has been speculation that toxic chemicals from plastic wastes can be transferred to the food chain and to wildlife (Arthur et al. 2008; Thompson et al. 2009; Thompson et al. 2004). These detrimental effects highlight the need for renewable, bio-based, biodegradable plastics in order to solve environmental and waste management problems of petro-plastics (DiGregorio 2009; Iwata 2015).

In 1926, Maurice Lemoigne, a chemist and bacteriologist, discovered that the bacterium *Bacillus megaterium* has the ability to produce the natural biopolyester, poly(3-hydroxybutyrate), which is abbreviated as PHB (DiGregorio 2009). In 1959, W. R. Grace and Company in the United States produced Polyhydroxybutyrate (PHB) for potential commercial applications (Baptist, J.N., US Patent No. 3225766, 1965). However, the low production efficiency along with the lack of suitable purification methods made the process economically inviable, resulting in the shut-down of the company.

Later, in 1970, Imperial Chemical Industries Ltd. (ICI/Zeneca BioProducts, Bellingham, UK) commercialized poly(3-hydroxybutyrate-*co*-3-hydroxyvalerate), abbreviated as (PHBV), under the trade name of Biopol™ (Holmes 1985; Chanprateep 2010). In 1996, Monsanto bought the technology and afterward Metabolix Inc. In 2008, Metabolix Inc. reported that the combined production of Biomass Energy and PHA to achieve PHA at a value of 20% of dry cell weight from switchgrass, 75% of which could be recovered. Hence, if switchgrass yields are between10 and15 tons per acre, 1.5 to 2.25 tons of PHA per acre could be produced (Chanprateep 2010; Somleva et al. 2008). Increasing the availability of raw renewable materials and expansion of using biodegradable plastics resulted in the growth of PHA market. According to the global PHA market in 2016 (estimated US $73.6 million), it is predicted to reach US $93.5 million in 2021 with a compound annual growth rate of 4.88% (Kourmentza et al. 2017; MarketsandMarkets 2017).

PHAs with about 150 different monomer composition have been described. Different monomer compositions convey different physical/mechanical and thermal properties to the polymers, and thus determine their potential applications (Hazer and Steinbüchel 2007; Jendrossek and Handrick 2002). Among different types of thermoplastics, they are well known as they are biodegradable, biocompatible, piezoelectric, and non-toxic (Iftikhar and Jamil 2016; Masood et al.

2015). In this thesis, microbial growth and production of medium chain length PHAs (mcl-PHAs) by *Pseudomonas putida* LS46 grown on octanoic acid and under oxygen-limited conditions are modeled in the batch mode. The objective of this thesis was to describe PHA biosynthesis during a more efficient and low-cost fermentation process (low dissolved oxygen environments, low-cost substrate), which will assist in the development of a strategy for industrial-scale production. The role of each variable (limiting substrate concentration, initial biomass concentration, and time), under the experimental conditions was determined. This was very important for the optimization mcl-PHA production processes. The following sections (1.2-1.3) present the importance of PHA as a bioplastic. The production processes, bottlenecks for industrial-scale production, and how modeling may be used to assist in the design of large-scale fermentation processes will be presented. The various approaches, benefits, and challenges of modeling PHA production will also be discussed.

1.2. PHA Production

1.2.1. PHA as an Alternative Polymer for Plastic Materials

PHAs are elastomeric polyesters (polyoxoesters) that usually made up of 600 to 35,000 (R)-hydroxy fatty acid monomers and can be synthesized by various types of microorganisms (Vidhya and Aasha 2018). Once nutrient supplies (for instance nitrogen, phosphorus, or oxygen) become limiting, it is beneficial for bacteria to store the excess carbon inside the cells. This happens through polymerizing soluble carbon intermediates into insoluble molecules such as PHAs (Madison and Huisman 1999).

Although over 300 different microorganisms have the ability to biosynthesize PHAs, only a few bacteria, such as *Alcaligenes eutrophus*, recombinant *E. coli, Azotobacter vinelandii*, several strains of methylotrophs, recombinant *Al. eutrophus*, *Pseudomonas oleovorans*, recombinant

Klebsiella aerogenes, and *Alcaligenes latus* can produce sufficient PHA in a relatively short time period (reviewed by (Lee 1996b). In choosing the microorganism for the industrial production of PHA, various factors must be considered, such as stability of the organism, the ability of the bacterial cell to use cheaper and more readily available carbon sources (e.g. industrial by-products or agricultural wastes), the type, quality and quantity of PHAs, the rate of growth and polymer synthesis, the cost of the components of the medium, as well as the cost of the downstream processes (Babel and Steinbüchel 2001).

PHAs are mainly classified into two groups: short chain length PHA (scl-PHA) with maximum five carbon atoms, and medium chain length PHA (mcl-PHA) contain 6-14 carbon atoms. Longer chain monomers (lcl-PHA > C_{14}) have also been reported (Zinn et al. 2001; Lee 1996a). Whereas most bacteria synthesize either mcl- or scl- monomer units, PHAs containing both scl- and mcl- monomers have also been recognized in some bacteria (Chen et al. 2001).

Medium chain length PHAs behave as elastomers. They have low crystallinity (20–40%) and also do not break easily (extension to break of 300–450%) (Keshavarz and Roy 2010; Marschessault et al. 1990). In addition, because of the natural origin and enhanced biocompatibility of PHAs, they are very attractive materials for biomedical purposes. A few companies, such as P&G (US), Metabolix (US), TEPHA (US), produce PHAs in the form of screws, films, pins, sutures, and other devices. However, PHAs have variable subunit compositions, physiochemical and thermal properties, and different degradation rates. The distance between the ester linkages in the polymer backbones or the length of the pendant groups can affect the properties of PHAs (Misra et al. 2006; Williams et al. 1999). In the near future, it is predicted that PHAs, with their various properties will displace some petro-plastics such as polypropylene and polyethylene (Novak et al. 2015; Chen 2009).

1.2.2. PHA Synthesis Pathways

1.2.2.1. Short Chain Length (scl-) PHAs

Scl-PHAs are synthesised from glucose, long chain fatty acids (LCFAs), and volatile fatty acids (VFAs) via a three-enzyme pathway in which acetyl-CoA is the precursor. Acetyl-CoA molecules are produced from Entner-Doudoroff, β-oxidation, or pentose phosphate pathway and they are condensed into acetoacetyl-CoA (via the enzyme β-ketothiolase). Then, acetoacetyl-CoA is reduced to 3-hydroxybutyrl-CoA by acetoacetyl-CoA reductase and is subsequently polymerized into PHB through a PHA synthase enzyme (PhaC). In this step, nicotinamide adenine dinucleotide phosphate (NADPH) play the role of the electron donor, including *C. necator*. In *C. necator*, acetoacetyl-CoA is reduced to (R)-3-hydroxybutyryl-CoA by consuming the NADPH and regenerating $NADP^+$. Production of PHBV depends on condensation of propionyl-CoA with acetyl-CoA. Propionyl-CoA is produced from succinyl-CoA in the methylmalonyl-CoA pathway. Activation of propionate can be via β-oxidation of odd chain length fatty acids, or propionyl-CoA synthetase (Blunt 2018; Sudesh et al. 2000; Budde et al. 2010; Grousseau et al. 2013; Madison and Huisman 1999).

1.2.2.2. Medium Chain Length (mcl-) PHAs

Mcl-PHAs are synthesized via two metabolic pathways: 1) *de novo* fatty acid biosynthesis from carbon substrates that are structurally unrelated to the 3-hydroxyalkanoate subunits in PHA polymers (such as acetate, glycerol, glucose), and 2) the fatty acid β-oxidation pathway, which catabolizes carbon sources that are structurally related to the 3-hydroxyalkanoate subunits in PHA polymers (like alkanes and fatty acids). Synthesis of mcl-PHA from structurally unrelated carbon substrates is a reductive process that depends on successive condensation of acetyl-CoA precursors into 3-hydroxyacyl-ACP monomers. It consists of two reactions that utilize NADPH as the

electron donor. The composition of mcl-PHA synthesized via the *de novo* pathway does not specifically rely on the substrate and usually has monomer composition of mainly C10 and C8, with small amount of C14:1, C14, C12:1, C12 and C6 (Blunt 2018; Prieto et al. 2016; Eggink et al. 1992; Huijberts et al. 1992; Madison and Huisman 1999).

Synthesis of PHA from alkanes and fatty acids is a catabolic process. Through it, enoyl-CoA, hydroxyacyl-CoA, and 3-ketoacyl-CoA are converted to (R)-3-hydroxyacyl-CoA by the enzymes 1) trans-enoyl-CoA hydratase (PhaJ); 2) epimerase; and 3) R-specific ketoacyl-CoA reductase (FadG), respectively. The process is an oxidative process, and one $FADH_2$ is produced from oxidation of acyl-CoA to enoyl-CoA. NADH may also be produced from oxidation of (S)-3-hydroxyacyl-CoA to 3-ketoacyl-CoA (depending which intermediate is incorporated by PhaC) (Blunt 2018; Lageveen et al. 1988; De Waard et al. 1993; Hoffmann and Rehm 2004).

1.2.3. Bottlenecks in Industrial Production of PHA

Although PHAs have an extensive range of applications, their main drawback is related to the high cost of production. About 40–48% of the total cost of the process is ascribed to raw materials. Employing industrial by-products or waste streams (such as waste plant oils, agriculture feedstock, or wastewater) as raw materials is one of the main promising alternatives to reduce this cost. However, new technological advances are required to facilitate the employ of waste streams as substrates on pilot and industrial scales (Rodriguez-Perez et al. 2018; Mozejko-Ciesielska and Kiewisz 2016; Choi and Lee 1997; Schmidt et al. 2016; Narodoslawsky et al. 2015).

In addition to the price of the raw materials, the substrate-specific yield (g or mol PHA/g or mol carbon source), the volumetric production rate (productivity = Q_v, g PHA L^{-1} h^{-1}), and cell mass yield (g PHA/g cell dry weight), and downstream processing costs greatly influence the cost of production (Choi and Lee 1999). Hence, along with applying low-cost carbon sources,

improving productivity through mode of bioreactor operation and cultivation techniques is also required (Blunt et al. 2018; Kaur and Roy 2015).

1.2.4. The Role of Oxygen-limited Conditions in PHA Production

Synthesis of mcl-PHAs is an aerobic process and maintaining an adequate amount of dissolved oxygen (DO) specifically in large-scale bioreactors is a costly process. Oxygen mass transfer of is usually rate-limiting and significantly affects the productivity of the process. To rise the driving force, operating bioreactors at an elevated pressure or using pure oxygen has been employed (Blunt 2018; Maclean et al. 2008; Gao et al. 2016; Garcia-Ochoa and Gomez 2009; Follonier et al. 2012). However, the oxygen volumetric mass transfer coefficient decreases at high pressure (Lopes et al. 2013). Both methods are intended to lengthen the growth phase prior the mass transfer of oxygen becomes rate-limiting to increase productivity (Blunt 2018).

It has been reported that in low DO concentrations, the short chain length PHA content increased in several microorganisms grown on different cultures (Blunt 2018; Kshirsagar et al. 2013; Senior et al. 1972). Pratt et al. (2012) has reported that under low DO conditions by using mixed microbial cultures, PHA production increases in comparison with that in high DO conditions. Blunt et al. (2017) observed that maintaining DO at 1-5% can increase mcl-PHA production significantly. Further decreases in DO almost did not affect the growth, yet improved the PHA production yield. The productivity was higher than its value by applying NH_4 limitation. Therefore, manipulation of the bioreactor oxygen transfer rate during the PHA accumulation stage can be a useful approach to increase the PHA production yield in fed batch and continuous process.

1.3. Modeling

1.3.1. Why Modeling?

Mathematical modeling is a powerful tool for control and optimization of microbial metabolism for product synthesis, as well as for modeling the metabolism of individual cells or the whole cell populations. Linking mathematical modeling with experimental results may not only reveal new aspects of microbial physiology but may also improve our knowledge to design more effective processes, which can release the full genetic/biochemical potential of the producing strains and greatly enhance the large-scale productivity (Novak et al. 2015). A mathematical model refers to a description of a system by considering mathematical concepts to properly explain a system or to investigate the impacts of various components and to establish predictions on patterns of behaviour (Abramowitz 1968; Ningthoujam et al. 2018)

The complexity of cell reactions and the segregated nature of biological systems are cumbersome for mathematical modeling in the bioengineering field. There is not any mathematical model that can be used to describe all features of industrial scale fermentation processes or producing strains. Different requirements need to be addressed for modelling process with different conditions. Thus, it is necessary to adapt the modelling methods appropriately to the actual processes (Novak et al. 2015).

1.3.2. Different Modeling Approaches

Model theory divides models into several groups: black/grey/white-box, nonverbal/verbal, continuous/discrete, explanatory/descriptive, structured/unstructured, segregated/distributed (non-segregated), mathematical/nonmathematical, and deterministic/stochastic. The combinations of the aforementioned models are also classified into dynamic, kinetic, cybernetic, and logistic models. In general, a specific model derived from biological systems can be linked to more than

one class. Highly variable types of models are used to express biotechnological process regarding mass transfer, cultivation techniques, metabolic network reaction kinetics, and microbial growth kinetics (Novak et al. 2015). In the following section, some of the models utilized in modeling microbial growth and PHA production are outlined.

1.3.2.1. Formal Kinetic (Unstructured and Low-structured) Models

In systems involving (bio)chemical reactions, kinetic modeling can be defined as mathematical description of changes in properties of the system over time (Dubitzky et al. 2013). Formal kinetic unstructured models focus on the kinetic relationships between substrate (S), biomass (X), and product (P). Although these models do not include metabolic reactions, they are still widely utilized due to their simplicity. The most popular unstructured, kinetic expression

$$\mu = \mu_{max} \frac{S}{S + K_s} \qquad \text{Equation 1}$$

employed today is the Monod equation (Equation 1) ((Novak et al. 2015); Moser (1985) and references therein).

where μ is specific growth rate (h^{-1}), μ_{max} is the maximum specific growth rate (h^{-1}), S is the limiting substrate ($g\ L^{-1}$) and, K_s is the substrate saturation constant ($g\ L^{-1}$). By considering the definition of specific growth rate (Equation 2, t is time (h), X is biomass concentration ($g\ L^{-1}$)), Equation 1 can also be written as follows (Equation 3) (Dhanasekar et al. 2003):

$$\frac{dX}{dt} = \mu X \qquad \text{Equation 2}$$

$$\frac{dX}{dt} = \mu_{max} \frac{S\,X}{S + K_s} \qquad \text{Equation 3}$$

When unstructured models cannot describe the system, low-structured models, based on formal kinetic principles, are employed. In low-structured models, biomass, a few intracellular metabolic reactions, and extracellular molecular species are involved, without genetic regulations.

Different models have been developed based on various substrates, strains, cultivation conditions, mutants and kinetics (Novak et al. 2015). For instance, Raje and Srivastava (1998) investigated the PHB production by *Alcaligenes eutrophus* under nitrogen-limited conditions. In this system, the specific growth rate μ was modeled with a linear combination of the Monod and Sigmoidal growth kinetics, additionally corrected with inhibition terms according to a high N/C, proposed by Luong (1985).

1.3.2.2. High-structured Models

Metabolic pathways and their genetic regulations are considered in this type of models. They require sufficient knowledge regarding metabolic pathways for the microorganisms. Although it is challenging to separate low-structured and high-structured models of microbial systems, genome-scale metabolic models belong to the high-structured ones. They aim to have the same number of reactions that exist in the real systems. In fact, it is not possible to verify which type of mathematical models is the best for a specific PHA biosynthesis due to the influence of cultivation condition, metabolism, genetic engineering, bioreactor structure, etc. It seems that the unstructured and low structured models are valid enough for standard bacteria cultivations, while complex multi-substrate cultivations need more advance modeling structure (Novak et al. 2015).

1.3.3. Microbial Growth Kinetics

The relationship between the substrate concentration (S) and the specific growth rate (μ) is a precious tool in bioengineering. Derived rate laws, referred to as theoretical models, are used to portray this relation (Okpokwasili and Nweke 2006). The model of Blackman, one of the earliest growth models, assumes that uptake and growth rate are proportional to substrate concentration at its concentrations. Conversely, at high substrate concentrations, growth rate is not dependent of the substrate concentration (some other nutrient or intracellular factor is limiting in this case)

(Koch 1997; Blackman 1905). When substrate concentration is more than the half-saturation coefficient (K_b), the Blackman model (Equation 4) has a extreme shift from the first order to the zero-order ((Mrwebi 2004; Neeleman 2002); Moser (1985) and references therein).

$$\mu = \mu_{max} \frac{S}{K_b} \qquad \text{if } S < K_b$$

$$\mu = \mu_{max} \qquad \text{if } S \geq K_b \qquad \text{Equation 4}$$

As indicated in section 1.3.2.1 Monod developed the non-linear relationship between limited substrate concentration and specific growth rate (Equation 1). This relation is based on growth of *E. coli* at different concentrations of glucose. Monod's equation and the Michaelis-Menten equation have the same form, yet Michaelis-Menten equation has theoretical base, while Monod equation is empirical. The Monod model has high accuracy for simple substrates and pure cultures (Monod 1949; Contois 1959; Mahanta et al. 2014). The limitation of Monod model is that it does not consider that cells may synthesize the product or may need substrate, even if they are in the stationary phase, and not undergoing cell division as they do during the exponential growth phase (Raghuvanshi and Babu 2010). Monod relation also does not consider the lag phase. Therefore, in addition to the Monod equation, various models have been proposed to illustrate the microbial growth kinetic (Mahanta et al. 2014).

Hermann Moser developed a modified form of the Monod model. Moser improved the Monod equation through the use of a parameter, *n* (usually $n > 1$), which accounted for the adoption of microorganisms to stationary processes (for Monod equation *n* is equal to one) (Equation 5).

$$\mu = \mu_{max} \frac{S^n}{S^n + K_s} \qquad \text{Equation 5}$$

Where *n* is an adjustable parameter ((Mahanta et al. 2014); Moser (1985) and references therein.)

Aiba (Equation 6) and Andrews (Equation 7) models are other models to describe the microbial growth kinetic by considering the effects of substrate inhibition. Where $K_{I,S}$ is substrate inhibition constant ((Andrews 1968); Moser (1985) and references therein).

$$\mu = \mu_{max} \frac{S}{S + K_s} \exp\left(\frac{-S}{K_{I,S}}\right) \quad \text{Equation 6}$$

$$\mu = \frac{\mu_{max}}{\left(1 + \frac{K_S}{S}\right)\left(1 + \frac{S}{K_{I,S}}\right)} \quad \text{Equation 7}$$

1.3.4. Modeling PHA/PHB Synthesis

Different mathematical models have been established to improve the production of PHAs in bioreactors (Table 1.1; (Dhanasekar et al. 2003)). Heinzle and Lafferty (1980) presented a structured model for PHB production of *A. eutrophus* H16 (also known as *R. eutropha* H16 and *C. necator* H16) in nitrogen-limited batch cultures. Later, Raje and Srivastava (1998) modified a model for PHB synthesis by *A. eutrophus* B4383. Their mode was employed to simulate nutrient feeding profiles to improve the synthesis of PHB in a fed-batch mode.

Tohyama et al. (2002) upgraded models for PHB synthesis by introducing dissolved oxygen into their model. This model described the impacts of glucose, dissolved oxygen, ammonia (NH_3), and lactate concentrations on the dynamic behaviour of glucose and lactate concentrations, the cell mass production, and the PHB yield. It was recognized that the periodic change in DO concentration increased the PHB yield. Also, the optimal NH_3 concentration profile for efficient PHB production was found. Yu et al. (2002) worked on a kinetic modeling of the PHA production from volatile fatty acids, specifically butyrate, propionate, and acetate, by *R. eutropha.* The authors considered acid inhibitory on PHA biosynthesis and suggested butyric acid for polymer synthesis among the three acids.

Dias et al. (2008) presented a metabolic model for synthesis of PHA copolymers in mixed microbial cultures by using acetate and propionate as carbon sources. By comparing the metabolic fluxes of mixed cultures versus a pure culture of *C. necator*, they concluded that mixed microbial cultures are able to produce PHA more appropriate than pure cultures. Jiang et al. (2011) also employed mathematical modeling for PHA production with acetate, propionic acid, and acetate-propionate mixtures as carbon substrates. The dominate microorganism in this study was *Plasticicumulans acidivorans*, and the model was able to estimate the PHA composition as a function of the carbon source composition for propionate-acetate mixtures.

Horvat et al. (2013) established a mathematical model for synthesis of PHB in a multi-stage, continuous stirred tank reactor system with *C. necator* DSM545 as the production strain. Optimization of the system using mathematical models resulted in the PHB production enhanced from 2.14 g L^{-1} h^{-1} to 9.95 g L^{-1} h^{-1}. Mozumder et al. (2014) developed a mechanistic model for production of PHB by *R. eutropha*. The PHB inhibition in the fed-batch system followed a nonlinear relation under nitrogen-limited conditions. Mechanistic modeling uses theoretical knowledge of predictor variables, such as processes along with their interactions, to estimate the target variables. Mechanistic modeling are based on mathematical equations and equivalent to theoretical modeling (Carranza 2008).

Most of the published models are about the production of PHA or PHB by *A. eutrophus* and few models have been developed for production of PHAs by *Pseudomonas* species. Koller et al. (2006) developed a low structured mathematical model for poly-3-hydroxybutyrate (P3HB) production by *P. hydrogenovora* from whey permeate. Annuar et al. (2008) also presented a kinetic model for PHA synthesis by *P. putida* PGA1 using saponified palm kernel oil under nitrogen - limited conditions.

Table 1.1 Models for biomass and polyhydroxybutyrate (PHB) production.

Model	Equations	Reference
Monod	$X_t = X_0\,[exp\left(\frac{\mu_{max}\,S\,t}{K_s + S}\right)]$	(Dhanasekar et al. 2003)
Monod incorporated Leudeking–Piret (MLP)	$P_t = P_0 + \alpha\,X_0\,[exp\,(\frac{\mu_{max}\,S\,t}{K_s + S}) - 1] + \frac{\beta X_0}{\left(\frac{\mu_{max}\,S}{K_s + S}\right)}.[exp\,(\frac{\mu_{max}\,S\,t}{K_s + S}) - 1]$	
Logistic	$X_t = X_0.\exp(\mu t).[1 - \left(\frac{X_0}{X_m}\right).[1 - \exp(\mu t)]\,]$	(Dhanasekar et al. 2003)
Logistic incorporated Leudeking–Piret (LLP)	$P_t = P_0 + \alpha\left[\frac{X_0\,\exp(\mu t)}{\left[1 - \left(\frac{X_0}{X_m}\right)\,[1 - \exp(\mu t)]\right]} - X_0\right] + \frac{\beta X_m}{\mu}\,ln\,[1 - \left(\frac{X_0}{X_m}\right)[1 - \exp(\mu t)]\,]$	
Modified logistic	$X_t = \left[\frac{X_0^r \exp(\mu r t)}{[1 - \left(\frac{X_0^r}{X_m^r}\right)\,[1 - \exp(\mu r t)]]}\right]$	(Dhanasekar et al. 2003)
Modified logistic incorporated Leudeking–Piret (MLLP)	$P_t = P_0 + \alpha\,\{\left[\frac{X_0^r \exp(\mu r t)}{[1 - \left(\frac{X_0^r}{X_m^r}\right)[1 - \exp(\mu r t)]]}\right]^{\frac{1}{r}} - {X_0}^r\}$ $+ \frac{{X_m}^r}{\mu} \ln\,\{1 - \left(\frac{X_0^r}{X_m^r}\right)[1 - \exp(\mu r)]\}\,\beta$	
Moser	$X_t = X_0\,[exp\left(\frac{\mu_{max}\,S^n\,t}{K_s + S^n}\right)]$	----
Moser incorporated Leudeking–Piret	$P_t = P_0 + \alpha\,X_0\,[exp\,(\frac{\mu_{max}\,S^n\,t}{K_s + S^n}) - 1] + \frac{\beta X_0}{\left(\frac{\mu_{max}\,S^n}{K_s + S^n}\right)}.[exp\,(\frac{\mu_{max}\,S^n\,t}{K_s + S^n}) - 1]$	

1.4. Research Questions

In this thesis, the specific objective of this research will address the following questions:

I. Which model(s) is able to describe the microbial growth and production of mcl-PHAs by *Pseudomonas putida* LS46 grown on octanoic acid and under oxygen-limited

conditions in the batch mode? Empirical equations that had been proposed in the literature are used to model the data collected by Blunt (2018).

II. Which method and metric(s) can be used for calibrating and validating the model?

III. Do the selected model(s) adequately simulate the oxygen excess condition?

Chapter 2

Materials and Methods

2. Methodology

2.1 Data Collection and Analysis

The experimental data for microbial growth and biosynthesis of mcl-PHAs was acquired from the work of Blunt (2018). The biopolymer was produced by *Pseudomonas putida* LS46 under oxygen-limited conditions in the batch mode. The substrate for all experiments was octanoic acid. Since residual cell mass (X_r, Equation 8) was used for calculation of specific growth rate by Blunt (2018) to reflect cell growth, X_r has been employed for the modeling.

$$[X_r] = [X_T] - [X_{PHA}] = [X_T]\frac{(100 - \%_{PHA})}{100} \qquad \text{Equation 8}$$

The experiments were performed at 0%, 1%, 5%, 10%, and 40% dissolved oxygen (DO). As *P. putida* LS46 grew slightly slower and had a reduced PHA content in cultures containing 10% DO, the 10% DO condition was considered as oxygen excess. Obviously, the 40% DO condition was also considered as oxygen excess. Hence, only the data related to 0%, 1% and 5% DO was used for calibration and validation of the microbial growth and PHA production model. The data corresponding to 10% and 40% was employed to show that the model is only accurate under oxygen-limited conditions. The data used for modeling was also obtained from cultures when dissolved oxygen concentration became constant. Figure 2-1 shows dissolved oxygen concentration curve, octanoic concentration curve, growth curve, and PHA production curve for one data set for 0% DO. Before 7 h, dissolved oxygen concentration is not constant and after 11 h the system is under carbon limited conditions instead of oxygen-limited conditions. Therefore, the data from 7 to 11 h was used for modeling, and time 7 h was considered as time zero in modeling

this data set. The similar conclusions (based on DO curves and octanoic concentration curves) were drawn for all the data sets (0%, 1%, 5%, 10%, and 40% DO; see Appendix A).

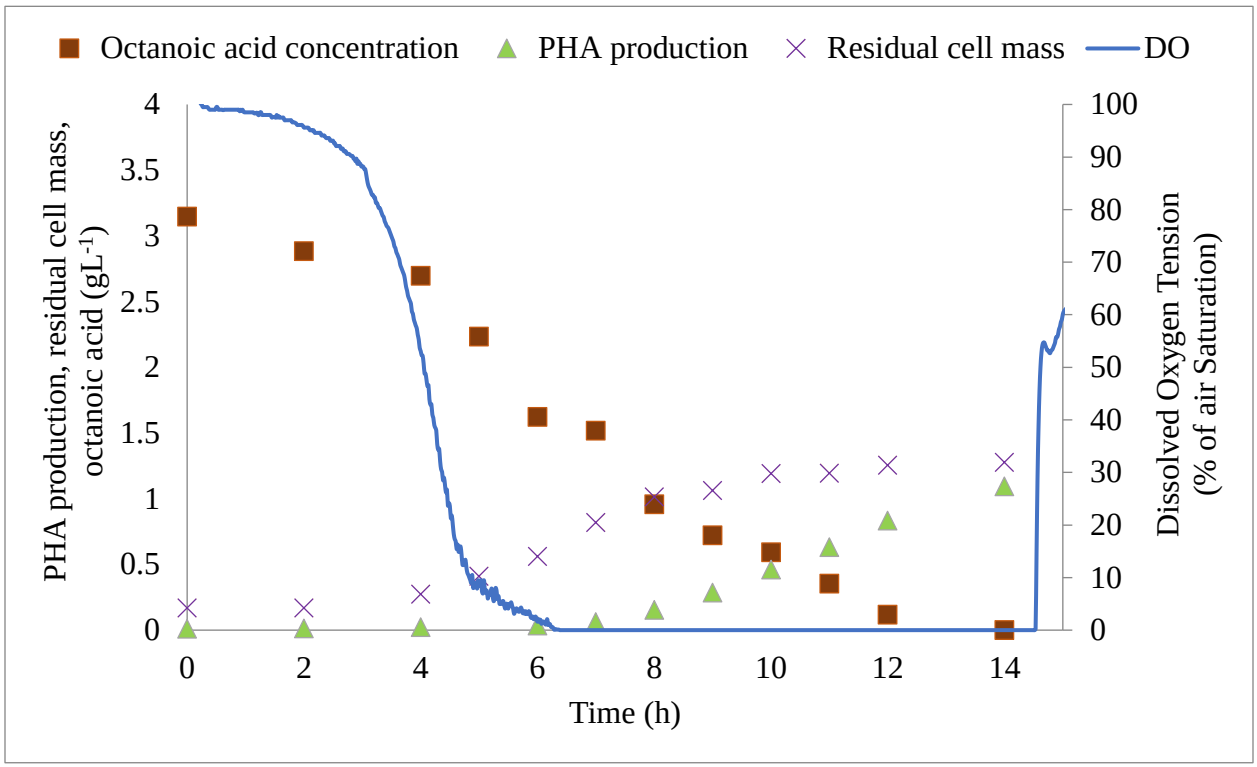

Figure 2-1 Representative DO, growth and PHA production curves from octanoic acid at 0% DO (Adapted from Blunt (2018)).

The data corresponding to 0%, 1%, and 5% DO were derived from two independent (duplicate) experiments. One data set for 0% and 5% DO were employed for calibrating parameters of the models, while the other data set for 0% and 5% DO, along with both sets of data for 1% DO, were used for validation of the model. Therefore, the validation is expected to show if the calibrated model has deviation from experimental data at the beginning, middle and/or the end of DO range, it would be obvious. The only exception was two data points (at the 1 h and 2 h time points) in the second set of data for 0% (Table 2.1). These two points always were used for validation the model, as at least one of them is not correct. Cell mass should increase during the

growth phase, but the data at 2 h shows a decrease in the cell mass. Perhaps the measurement of the cell mass at 2 h was faulty (making the data for this time point an outlier), or the data at 1 hr was greater than it should be, making the data for this time point an outlier. For choosing the two sets of data for calibrating the model, all possible combinations of the duplicate data sets were considered: (1,1), (2,2), (1,2), and (2,1). The experimental μ_{max} (0.578 ± 0.142) was the average of μ_{max} for the data corresponding to 0%, 1%, and 5% DO. Maximum specific growth rate was reported with three decimals as residual cell mass (gL^{-1}) was measured with three decimals. The error, 0.142, was the standard deviation of the experimental data.

Table 2.1 Residual cell mass and PHA production concentrations at different percentage of dissolved oxygen (Blunt 2018, data not shown).

Data set 1			**Data set 2**		
Time (h)	**Residual cell mass (gL^{-1})**	**PHA production (gL^{-1})**	**Time (h)**	**Residual cell mass (gL^{-1})**	**PHA production (gL^{-1})**
0% dissolved oxygen (0.000041 gL^{-1})					
0	0.819	0.061	0	0.766	0.117
1	1.012	0.153	1	0.812	0.189
2	1.063	0.285	2	0.802	0.311
3	1.191	0.461	3	0.988	0.481
4	1.194	0.631	4	1.025	0.631
5	---	---	5	1.185	0.870
1% dissolved oxygen (0.00007 gL^{-1})					
0	0.486	0.047	0	1.064	0.167
2	0.589	0.129	1	1.336	0.341
4	1.251	0.457	2	1.256	0.681
6	1.333	0.777	3	1.265	0.941
5% dissolved oxygen (0.00034 gL^{-1})					
0	0.556	0.026	0	0.828	0.038
1	1.037	0.077	1	1.176	0.215
2	1.274	0.220	2	1.560	0.285
3	1.396	0.428	3	1.688	0.453
10% dissolved oxygen (0.00068 gL^{-1})					
0	0.557	0.033	---	---	---
2	1.577	0.130	---	---	---
40% dissolved oxygen (0.00271 gL^{-1})					
0	2.401	0.152	0	0.287	0.011

1	1.168	0.082	1	0.241	0.009
2	2.208	0.167	2	0.495	0.015
---	---	---	3	1.194	0.038
---	---	---	4	1.765	0.080

2.2 Calibrating the Models for Microbial Growth and PHA Production

2.2.1 Model Evaluation

Different metrics, such as mean squared error (MSE), sum of squares error (SSE), and sum of absolute error (SAE) can be used to evaluate the model performance based on the residuals between simulated and measured values. The model evaluation should not be biased toward higher or lower residual values. Therefore, in cases where residuals are orders of magnitude different, multiple metrics have to be used to balance between them. In this study, it was decided to use SAE in Equation 9 for model evaluation, because all experimental datasets were in range [0, 1] or close to 1 and therefore residuals for a reasonable model are expected to be less than 1. In this case, SAE is preferred to SSE in Equation 10, because SSE is not sensitive to small error values in range [0, 1]. The same rationale is applied to MSE in Equation 11.

$$\text{SAE} = \sum_{i=1}^{N} \left| X_i - \widehat{X}_i \right| \qquad \text{Equation 9}$$

Where X_i is experimental data and $\widehat{X}_i$ is estimated data by the model. The ideal value for SAE is zero.

$$\text{SSE} = \sum_{i=1}^{N} (X_i - \widehat{X}_i)^2 \qquad \text{Equation 10}$$

$$\text{MSE} = \frac{1}{N} \sum_{i=1}^{N} (X_i - \widehat{X}_i)^2 \qquad \text{Equation 11}$$

The ideal value for SSE and MSE is zero.

2.2.2 Model Calibration

2.2.2.1 Concept of Model Calibration and Validation

Model calibration is the process of adjusting a set of input parameters/variables of a model that affect the model performance to maximize the resulting agreement between the simulated output and the measured data. Model validation quantifies the confidence in capability of a calibrated model to simulate data that was not used for the model calibration (Trucano et al. 2006).

2.2.2.2 Manual Model Calibration versus Automatic Model Calibration

In manual calibration, the modeler selects a subset of model parameters based on a guideline and runs the model to compare the simulated values with the available data. In the next step, the modeler changes one parameter value and runs the model again to compare the results. This step is iterated until sufficient goodness of fit is achieved (Sin et al. 2008). The manual calibration (trial and error) is subjective, tedious and time consuming (Sin et al. 2008). Automated calibration, a technique to reduce uncertainties related to the user's subjectivity, uses a computer code that involves an optimization algorithm applied to optimize a metric defined based on the statistical knowledge of the model response compared to the measured data and excludes intuition (Kresic 2006).

2.2.2.3 Local versus Global Optimization

Local optimization methods numerically or analytically estimate the derivative of the objective (response) function to search for an optimal solution in the neighborhood of an initial solution (Tolson and Shoemaker 2007). They converge fast when the initial solution is close to a local solution, but they may fail to converge on complex problems with many decision variables and nonlinear response (objective) functions (Van Hentenryck et al. 1997). These methods are designed to search for local optimum. To search for the global optimum with local optimization

methods, they need to be restarted at multiple initial solutions. Once an algorithm run converges, another run with different initial solution which is randomly chosen needs to be started. If the maximum function evaluation limit is not achieved, or if restarting the local method does not considerably improve the solutions, this procedure must be repeated (Tolson and Shoemaker 2007). In contrast, global optimization algorithms do not require the information about the derivative of the objective function and have the ability to search globally for the optimal solution. They generate a single solution or a population of solutions, evaluate them, and decide which solution(s) should be evolved for the next generation of the solutions.

2.2.2.4 Population-based versus Single Solution-based Optimization

Heuristic optimization algorithms search good feasible solutions through the decision space and archive high-quality solutions. They are applied when the computational budget is limited and/or the complexity of the problem does not allow to use exact solution approaches such as the derivative-based optimization approach.

In algorithms that can find the exact solution, time efficiency is the primary factor for an appropriate method. But in heuristic algorithms, how fast the solutions can be reached and how close do they come to being optimal are the two main factors that indicate the success/failure of the algorithm (Asadzadeh and Tolson 2013; Rardin and Uzsoy 2001).

One classification for heuristic algorithms is single solution vs. population-based solutions. In single solution algorithms such as the simulate annealing algorithm the optimizer perturbs (evolves) a single solution at a time, while in the population-based solutions such as the genetic algorithm a population of (multiple) solutions are evolved at the same time (El Yafrani and Ahiod 2016). Single solution based methods are exploitation oriented and they intensify the search in

local space, While population based approaches are exploration oriented and have a better diversification to search in the whole area (Talbi 2009).

2.2.2.5 Multi-objective versus Single Objective Optimization

Optimization algorithms can be classified as multi-objective and single objective. Multi-objective optimization problems do not have a single optimal solution. They rather have a set of non-dominated solutions that are often referred to as tradeoff or pareto solutions. If x_1 and x_2 are solutions of an algorithm, x_1 dominates x_2 in case x_1 is not worse than x_2 for all objective functions ($f_i(x_1) \leq f_i(x_2), i = 1,...,m$) and at least for one objective is better than x_2 ($\exists k \in [1,...,m] : f_k(x_1) < f_k(x_2)$). Solutions x_1 and x_2 are called non-dominated if x_1 is better than x_2 for one criterion, but x_2 is better than x_1 for another one. Non-dominate solutions are also named Pareto solution (PS) and their map in the objective space is often called Pareto front (PF) (Kavunnikova et al. 2019).

In case of conflict between objectives (multi-objective optimization problems), no single solution can be found to minimize all objectives simultaneously; instead, there is a set of solutions without any priority to each other (Asadzadeh and Tolson 2013). The aim of solving such a multi-objective problem is finding the trade-off between objectives. High quality estimates include points that are as close to the actual trade-off as possible and as broadly spread out as possible (Asadzadeh and Tolson 2009).

Multi-objective heuristic optimization algorithms have an archiving procedure that is usually based on a proximity measure of solutions that prefers results dominated by fewer other solutions (Asadzadeh and Tolson 2013). These algorithms also lose their performance because of dominance resistance when the number of objectives increases, therefore they need to be equipped with a specialized solution archiving strategy (such as epsilon archiving) (Sahraei et al. 2019).

Some of the well-known multi objective algorithms are: Epsilon Dominance Multi-objective Evolutionary Algorithm (Ɛ-MOEA) (Deb et al. 2003), Epsilon Dominance Nondominated Sorted Genetic Algorithm-II (Ɛ- NSGAII) (Kollat and Reed 2005), elitist non-dominated sorting evolution strategy (ENSES), multi-objective differential evolution algorithm (spMODE-II), multi-objective particle swarm optimization (MOPSO) and Pareto Archived Dynamically Dimensioned Search (PA-DDS) Algorithm (Asadzadeh and Tolson 2011, 2013; Asadzadeh et al. 2014).

2.2.2.6 PA-DDS Introduction

MATLAB optimization package, PA-DDS algorithm is a single-solution based heuristic multi-objective optimization algorithm, that archives all non-dominated solutions found during the search (Asadzadeh et al. 2014). The PA-DDS algorithm has three sub-algorithms: solution perturbation, selection, and archiving non-dominated solutions. Initially, PS and its map to the objective space PF are empty sets ($PS^a=Ø$, $PF^a=Ø$). For i = 1, …, q initial solutions, x is generated randomly within the decision variable boundaries (x^{min} and x^{max}) and f(x) objectives are calculated and are used to update PS^a and PF^a by the archive sub-algorithm. In the next step, x^{curr} is selected from PS^a using a selection metric for example the crowding distance or the hypervolume contribution. For i = 1 , … , NFE-q (NFE computational budget) p is calculated by Equation 14 and is used in calculating x^{new} by solution perturbation algorithm. If x^{new} is a new non-dominated solution or a dominating solution, it will be selected for generating the next solution; otherwise, one of the currently archived solutions will be selected to generate the next solution.

$$x = U\,(x^{min}, x^{max}) \qquad \text{Equation 12}$$

$$f(x) = (f_1(x),\ldots,f_m(x)) \qquad \text{Equation 13}$$

$$p = \frac{1 - \ln(i)}{\ln(NFE - q)} \qquad \text{Equation 14}$$

PA-DDS perturbs all decision variables in the beginning of the search and dynamically reduces the number of perturbed decision variables as the search progresses toward the end of the computational budget. The probability of selecting a decision variable for perturbation follows Equation 14. The perturbation for each decision variable follows a Normal distribution centered at the current value of the decision variable. The only parameter of PA-DDS is the perturbation size that determines the standard deviation of this Normal distribution (Asadzadeh and Tolson 2013).

2.2.2.7 Calibration and Evaluation Method

Kinetic models described in

Table 1.1 were calibrated to the experimental data using PA-DDS. PA-DDS is an efficient multi-objective optimization algorithm that adjusts its optimization behaviour to the users' computation budget. This algorithm is a single-solution based optimization algorithm, that archives all non-dominated solutions found during its global search and has the ability to estimate the trade-off between the objectives. In the first step, a MATLAB function is developed to calculate the model performance evaluation metrics for any set of model parameter values. In the second step, the achieved result is applied as initial solution in PA-DDS to accomplish better results and more importantly to estimate the trade-off between the objectives, if there is any. In comparison with some of the built-in MATLAB algorithms that are designed to search for local optimal solutions such as fminsearch and fmincon, PA-DDS is a global optimization algorithm, in that it searches globally to find the solution. This capability of PA-DDS as a global optimization algorithm, is not fully explored in in this study as the boundaries of decision variable were chosen close to the solutions that was obtained by MATLAB function (fminsearch). In case wider boundaries were selected in applying PA-DDS, the error would be higher than the error with using

fminsearch. Therefore, by using the boundaries close to fminsearch solutions in PA-DDS, not only the error was minimized but also the trade-off between the objectives was estimated. PA-DDS is not recommended for optimization with less than five parameters as local search methods are more efficient in those cases but single objective optimization algorithms such as fminsearch should be run multiple times to estimate the trade-off between the objectives.

Coefficient of Determination, R^2, may define as follows, if $\widehat{X}_i$ is the i^{th} estimated value by the predicted regression.

$$R^2 = \frac{\mathrm{var}(\widehat{X}_i)}{\mathrm{var}(X_i)} = \text{Variance explained by the model/ Total variance} \qquad \text{Equation 15}$$

A higher R^2 (close to 1) that in one model does not always indicate that the model is better. R^2 illustrates the spread of points around a regression line, and even shows that poorly (Achen 1982; King 1986). Thus, other metrics such as SAE, which is a better criterion for judging the models, should to be used along with R^2 for comparing the models. Lower value of SAE (closer to zero) shows a better model.

Chapter 3

Results and Discussion

3. Modeling Growth and Biosynthesis of PHA

In this chapter, one set of data among all possible combinations of the duplicate data sets ((1,1), (2,2), (1,2), and (2,1)) were chosen for calibration and validation of the models. Also, two models among MLP, Moser-LP, LLP and MLLP were selected for the data set, and the validity of the model under oxygen excess condition were investigated for 10% and 40% DO.

3.1 Kinetic Modeling

3.1.1 Data Set for Calibration and Validation

Table 3.1 shows MLP model parameters and the sum of the absolute error (SAE) or residual between the simulation model and the calibration and validation datasets when each of the four sets of data are used independently ([1,1], [2,2], [1,2], and [2,2]). The MLP model parameters were reported with 6 decimals (Table 3.1) as they affected the results very significantly, even with small deviations in the 6^{th} decimal place. For example, for data set [1,1], if these parameters considered with 3 decimal (0.397, 0.000, 0.035, 0.132) instead of 6 decimal (0.397111, 0.000100, 0.035056, 0.132300), SAE for calibration, validation, and calibration and validation would be 7.215, 24.499 and 31.714 instead of 0.925, 3.341, 4.266.

The difference in SAE (Table 3.1) was not significant among the four sets of data, which shows the experimental data sets were consistent. As data set [2,1] had the minimum SAE in both of the calibration and validation datasets, this dataset was chosen as the best data set for using MLP. The correlation coefficient (R^2) was almost the same for all four data sets. To calculate R^2, a minimum three data points were used; in cases where more data was available for the calculation, the R^2 value would be more representative of the linear relationship between the data points.

Comparing the calculated μ_{max} with the experimental value (0.578 ± 0.142) confirmed that MLP [2,1] with a calculated maximum growth rate of ~ 0.497 was a reasonably good fit.

Table 3.1 Kinetic parameter values of MLP model with different data sets.

	[1,1]	**[2,2]**	**[1,2]**	**[2,1]**
μ_{max}	0.397111	0.306625	0.301375	0.497074
K_s	0.000100	0.000100	0.000089	0.000200
α	0.035056	0.000000	0.000000	0.011609
β	0.132300	0.140000	0.126201	0.140165
Sum of absolute error of calibration	0.925	0.723	0.898	0.764
Sum of absolute error of validation	3.341	3.704	3.809	3.410
Sum of absolute error of calibration and validation	4.266	4.427	4.707	4.174
Minimum of R^2 in calibration and validation	0.61	0.62	0.62	0.62
Maximum of R^2 in calibration and validation	1.00	1.00	1.00	1.00

Table 3.2 indicates the Moser-LP model parameters with different data sets. The data set [2,1] had the minimum SAE in calibration and validation and was chosen as the best data set for applying Moser-LP. Comparing the calculated μ_{max} with its experimental value (0.578 ± 0.142) showed Moser-LP [2,1] with the maximum calculated growth rate of ~ 0.622 represents the experimental data closely.

Table 3.2 Kinetic parameter values of Moser-LP model with different data sets.

	[1,1]	**[2,2]**	**[1,2]**	**[2,1]**
μ_{max}	0.662800	0.606757	0.430100	0.621687
K_s	0.008155	0.009800	0.012600	0.001200
α	0.015200	0.000000	0.000000	0.030024
β	0.132200	0.139400	0.121251	0.137568
n	0.620600	0.634448	0.521500	0.845300
Sum of absolute error of calibration	0.913	0.697	0.813	0.756
Sum of absolute error of validation	3.529	3.788	4.262	3.399
Sum of absolute error of calibration and validation	4.442	4.485	5.076	4.155

Minimum of R^2 in calibration and validation	0.61	0.62	0.61	0.62
Maximum of R^2 in calibration and validation	1.00	1.00	1.00	1.00

Table 3.3 and Table 3.4 show the parameters of LLP and MLLP models with different data sets ([1,1], [2,2], [1,2], and [2,2]). The data set [2,1] and [2,2] with the minimum SAE in calibration and validation (6.805 and 7.041) were the best data sets for applying LLP and MLLP, respectively. R^2 was almost the same for all four data sets in the LLP model (Table 3.3), while it has the highest value for data set [2,2] in MLP model (Table 3.4).

Table 3.3 Kinetic parameter values of LLP model with different data sets.

	[1,1]	**[2,2]**	**[1,2]**	**[2,1]**
μ	0.073057	0.052100	0.073396	0.052100
α	1.286426	0.000000	0.036089	1.682443
β	0.130190	0.161359	0.156900	0.133000
Sum of absolute error of calibration	2.167	1.774	1.747	2.114
Sum of absolute error of validation	4.794	5.389	5.202	4.691
Sum of absolute error of calibration and validation	6.961	7.163	6.949	6.805
Minimum of R^2 in calibration and validation	0.62	0.63	0.62	0.63
Maximum of R^2 in calibration and validation	1.00	1.00	1.00	1.00

Table 3.4 Kinetic parameter values of MLLP model with different data sets.

	[1,1]	**[2,2]**	**[1,2]**	**[2,1]**
μ	0.300000	0.302500	0.300000	0.300000
α	0.137298	0.813626	2.200000	1.459157
β	254.993312	0.001000	0.842184	15.619789
r	0.001000	1.784400	0.361354	0.051772
Sum of absolute error of calibration	2.174	1.471	2.697	1.748
Sum of absolute error of validation	7.002	5.569	7.285	8.960
Sum of absolute error of calibration and validation	9.176	7.041	9.982	10.707
Minimum of R^2 in calibration and validation	---	0.76	0.68	0.66

3.1.2 Best model

Comparing SAE of calibration and validation of the selected dataset in MLP, Moser-LP, LLP, and MLLP models (4.174, 4.155, 6.805, and 7.041) in Table 3.5 revealed that the MLP and Moser-LP models represented the experimental data closely, while the LLP and MLLP with SAE 6.805 and 7.041 were inadequate in representing the experimental data. Comparing variance and R^2 in MLP and Moser-LP models (Table 3.6) also indicated that there were no significant differences between these two models in representing the experimental data. The highest difference in variance between these two models was 0.0077 (0.0700 - 0.0623) and the highest difference in R^2 was 0.00. These differences were not substantial and MLP and Moser-LP models could consider similar in representing the experimental data.

Table 3.5 Absolute error of the best data set in MLP, Moser-LP, LLP, and MLLP models.

	Sum of absolute error of calibration	**Sum of absolute error of validation**	**Sum of absolute error of calibration and validation**
MLP model (2,1)	0.764	3.410	4.174
Moser-LP model (2,1)	0.756	3.399	4.155
LLP model (2,1)	2.114	4.691	6.805
MLLP model (2,2)	1.471	5.569	7.041

Table 3.6 Statistical analysis of MLP and Moser-LP models.

	Variance (MLP model)	**Variance (Moser-LP model)**	**R^2 (MLP model)**	**R^2 (Moser-LP model)**
Calibration				
0% DO (Growth)	0.0012	0.0011	0.90	0.90
5% DO (Growth)	0.0268	0.0236	0.93	0.93
0% DO (PHA production)	0.0023	0.0022	0.99	0.99
5% DO (PHA production)	0.0006	0.0005	1.00	1.00
Validation				
0% DO (Growth)	0.0016	0.0018	0.88	0.88
5% DO (Growth)	0.0700	0.0623	0.87	0.87
1% DO (Growth)	0.0591	0.0605	0.77	0.77

1% DO (Growth)	0.0459	0.0444	0.62	0.62
0% DO (Growth)	0.0035	0.0037	---	---
0% DO (PHA production)	0.0006	0.0006	1.00	1.00
5% DO (PHA production)	0.0115	0.0119	0.98	0.98
1% DO (PHA production)	0.0086	0.0091	0.99	0.99
1% DO (PHA production)	0.0118	0.0121	0.99	0.99
0% DO (PHA production)	3.2E-07	8.00E-08	---	---

3.1.2.1 MLP model

According to Figure 3-1 there was a trade-off between the two error functions in MLP [2,1], meaning that by reducing the error either in the microbial growth or in the PHA, the error in the other factor increased. The x-y axis point (0.603, 0.161(•)) had a minimum error in the sum of absolute error of growth plus the sum of absolute error of PHA production. Figure 3-2 illustrates the calibrated data at the x-y axis point (0.603, 0.161), while Figure 3-3 and Figure 3-4 indicate validation of the model, MLP [2,1], at this point. MLP [2,1] showed the great fit for the calibrated data (SAE=0.764 (Table 3.5), Figure 3-2) and appropriate fit for the validated data (SAE=3.410 (Table 3.5), Figure 3-3 and Figure 3-4).

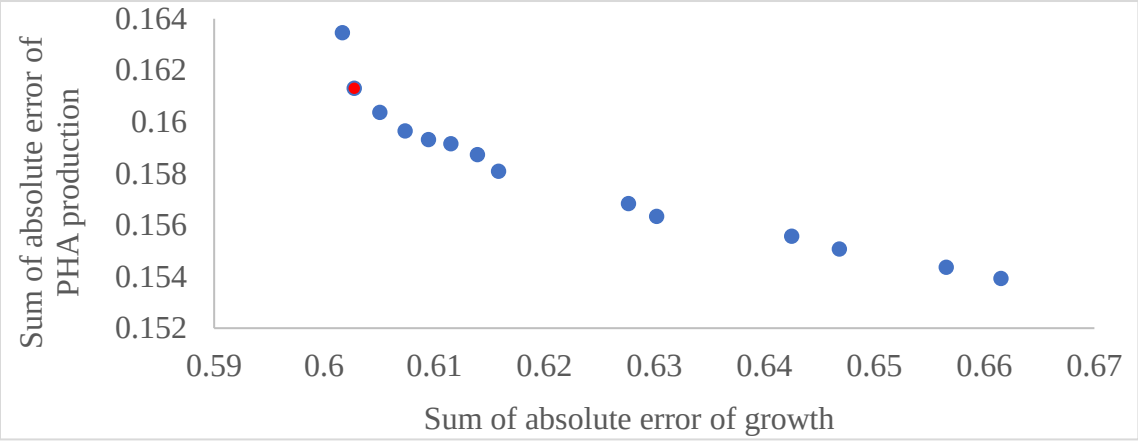

Figure 3-1 Trade-off between objectives in MLP [2,1].

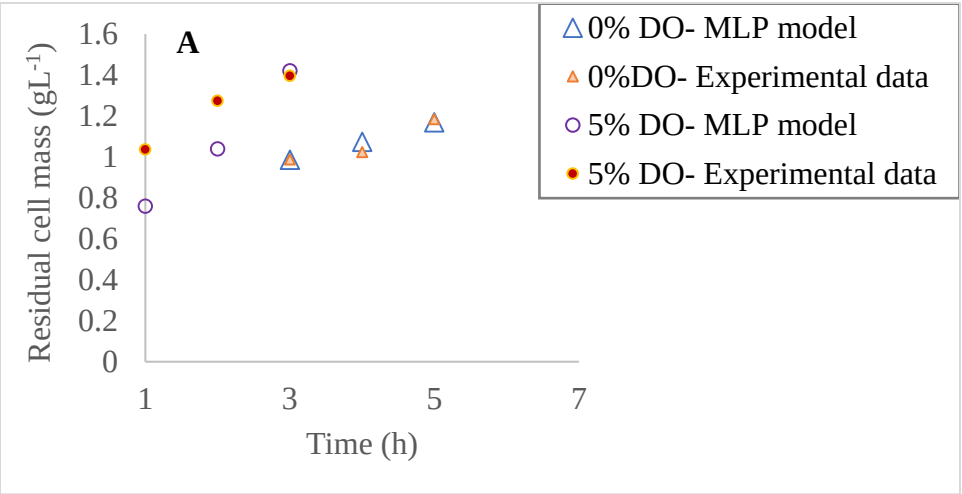

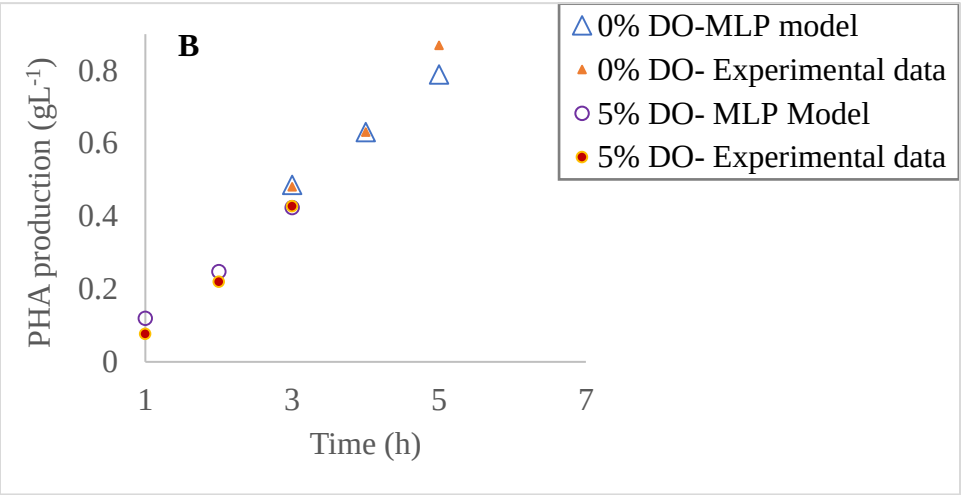

Figure 3-2 Calibration of A)growth and B)PHA production in MLP [2,1].

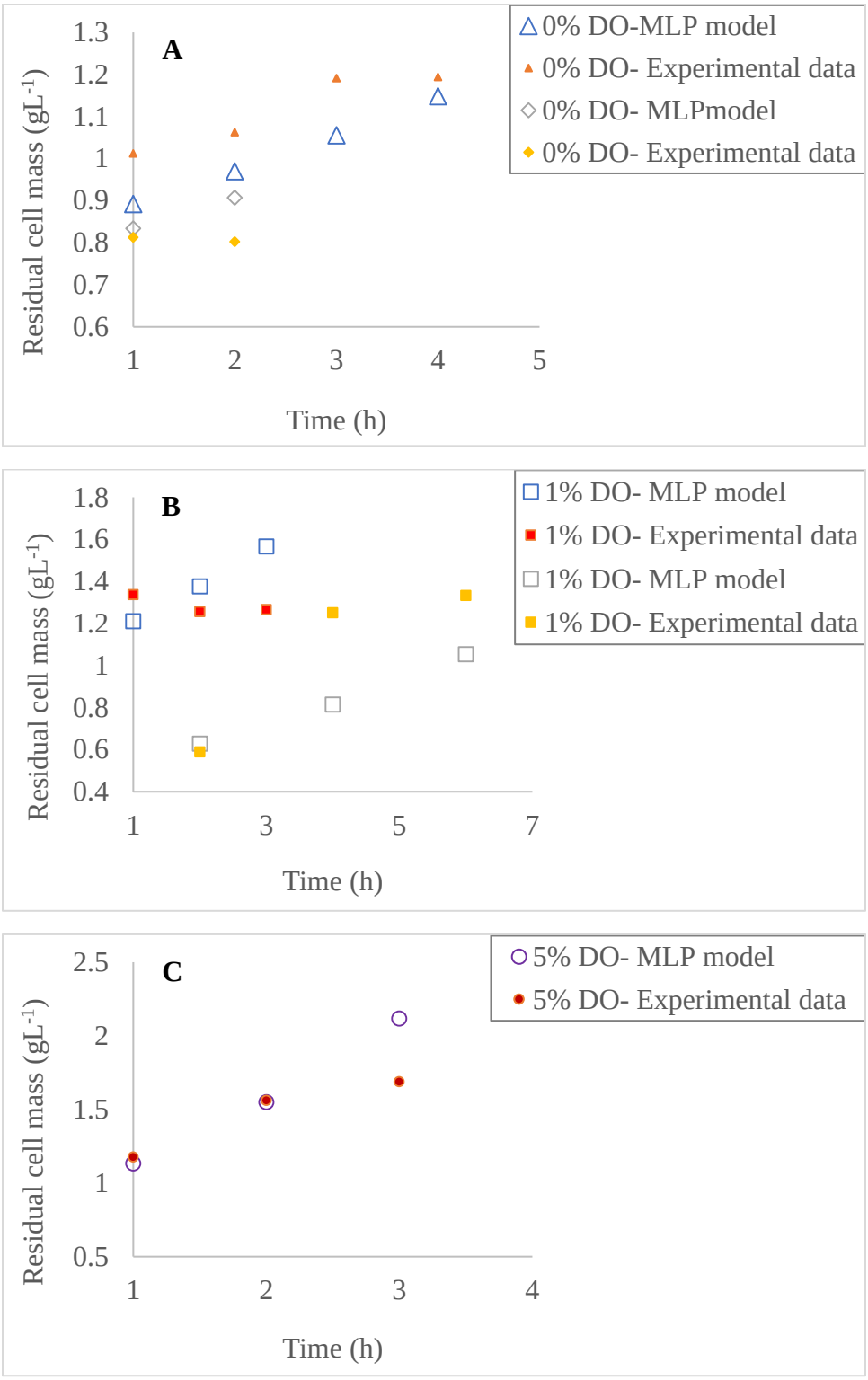

Figure 3-3 Validation of MLP [2,1] with growth data (A) 0% DO, B) 1% DO, C) 5% DO).

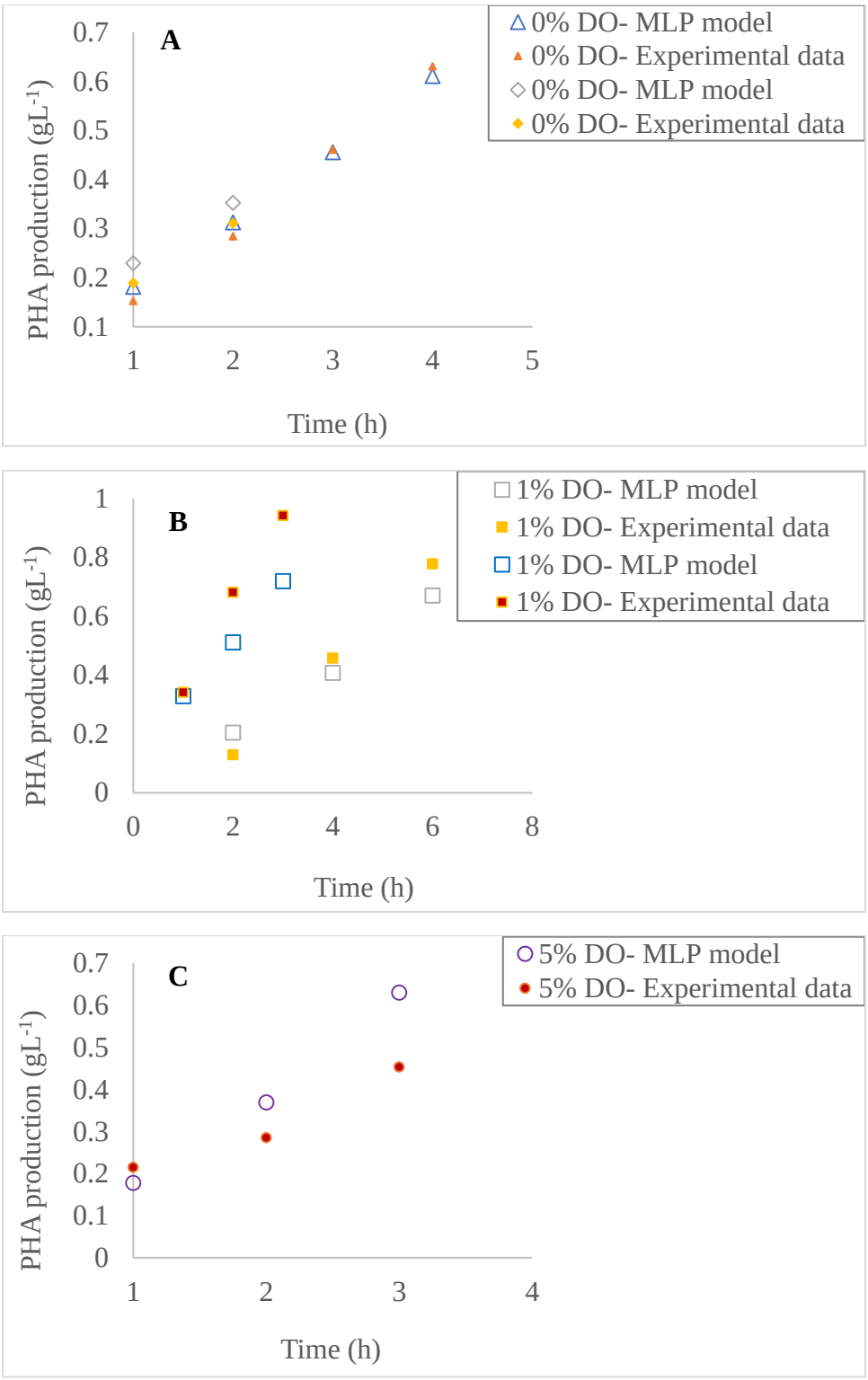

Figure 3-4 Validation of MLP [2,1] with PHA production data (A) 0% DO, B) 1% DO, C) 5% DO).

3.1.2.2 Moser-LP model

There is no trade-off between the error functions in Moser-LP [2,1]. There was a conflict between the error in microbial growth and the error in PHA production. The x-y axis point (0.596, 0.160) had a minimum error in sum of absolute error of growth plus the sum of the absolute error of PHA production. Figure 3-5 illustrates the calibrated data at the x-y axis point (0.596, 0.160), while Figure 3-6 and Figure 3-7 indicate validation of the model, Moser-LP [2,1], at this point. Moser-LP [2,1] showed the great fit for the calibrated data (SAE=0.756 (Table 3.5), Figure 3-5) and appropriate fit for the validated data (SAE=3.399 (Table 3.5), Figure 3-6 and Figure 3-7). The errors between the experimental data and the estimated data at different points, either its negative or positive, were not substantial.

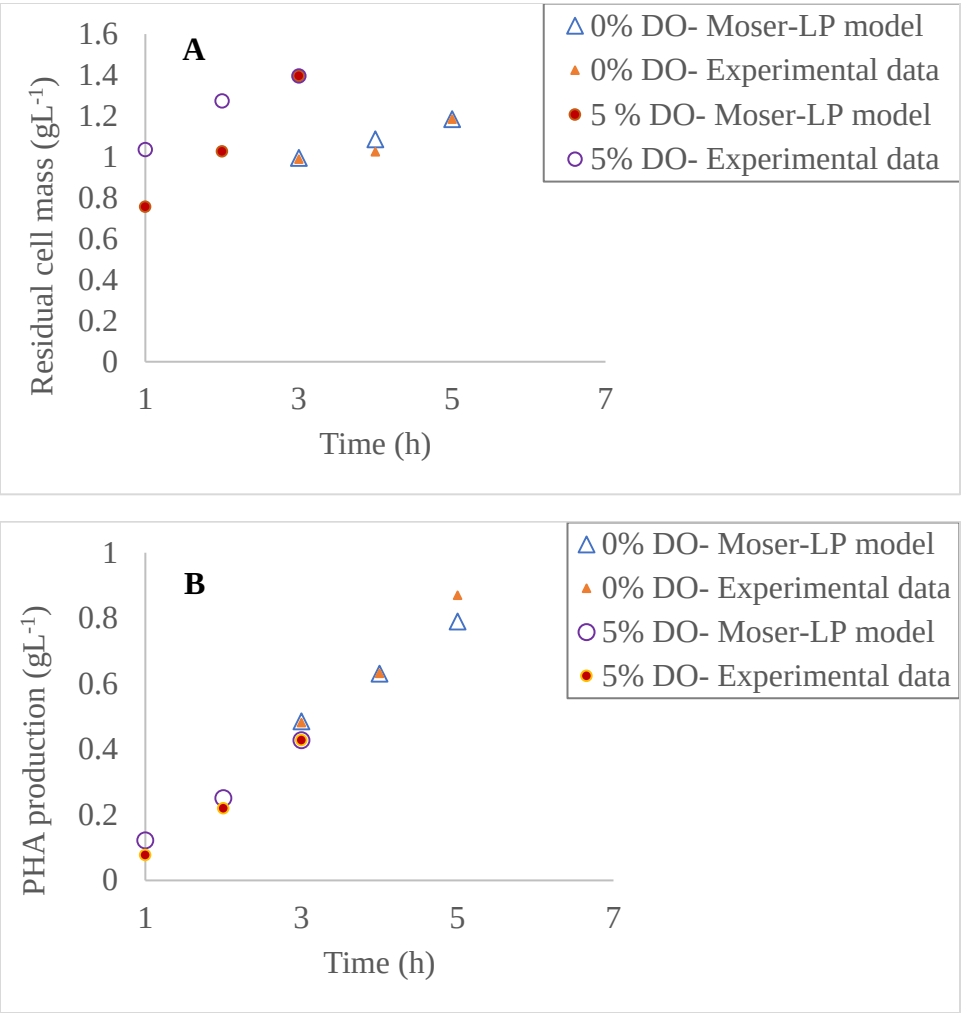

Figure 3-5 Calibration of A) growth and B) PHA production in Moser-LP [2,1].

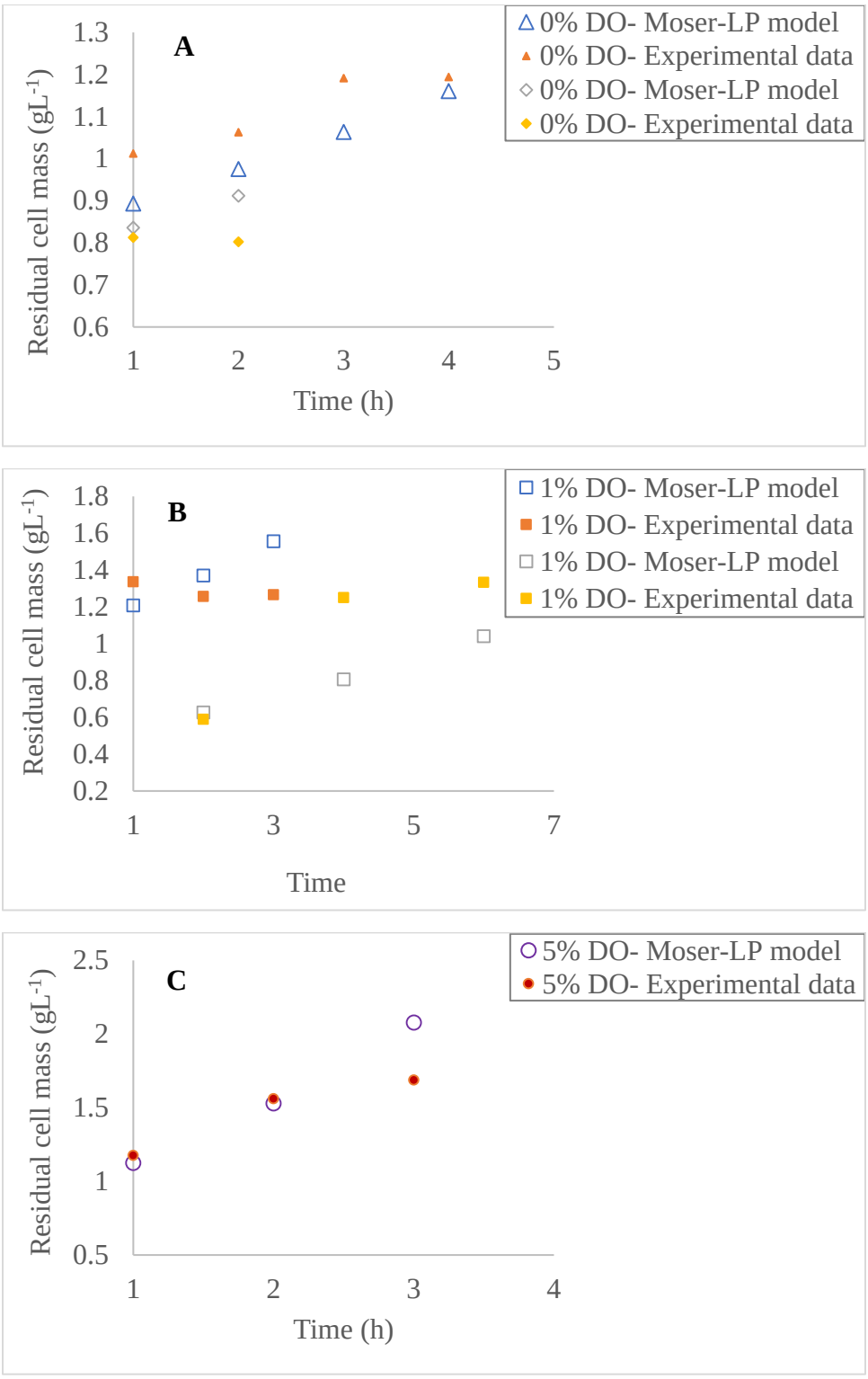

Figure 3-6 Validation of Moser-LP [2,1] with growth data (A) 0% DO, B) 1% DO, C) 5% DO).

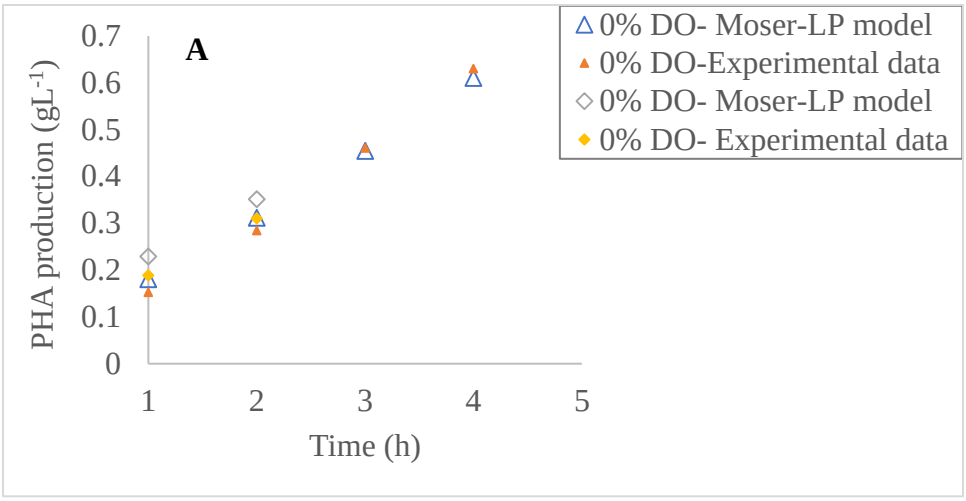

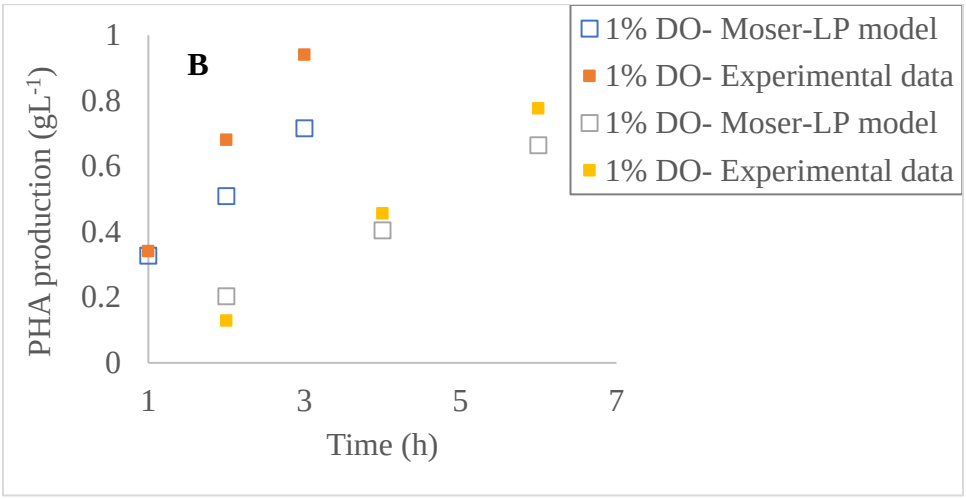

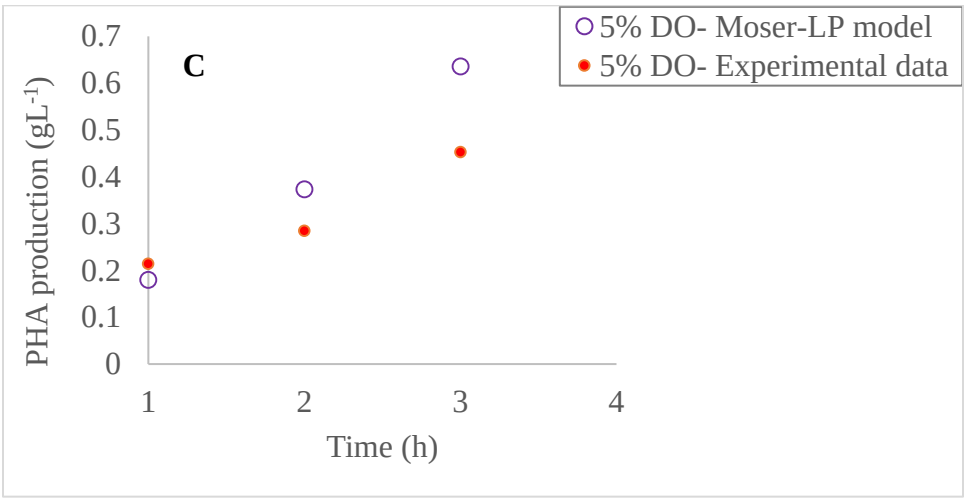

Figure 3-7 Validation of Moser-LP [2,1] with PHA production data (A) 0% DO, B) 1% DO, C) 5% DO).

3.2 Investigating the Validity of the Model under Oxygen Excess Conditions

The models MLP and Moser-LP under oxygen-limited conditions represent the experimental data closely. However, under oxygen-excess conditions (10% and 40% DO) PHA production was reduced in comparison with oxygen-limited conditions, and the models were inadequate in representing the experimental data (Figure 3-8 and Figure 3-9). This deviation was not very significant for the growth (except in one of the 40% DO data set), as growth did not change very considerably under the oxygen-excess conditions. The experimental data corresponding to the 40% DO data set had error as its growth curve had some outliers (point [1, 1.168] in Figure 3-9 and Figure 3-9, other outliers of the experiment were in conditions that oxygen concentration was not constant). These points were outliers as they showed decline in log-phase or very significant decrease in stationary phase. It seems the error of the experiment caused the deviation from the models. In case more data was available under oxygen-excess conditions for growth, the reason of the deviation from the models would be clearer.

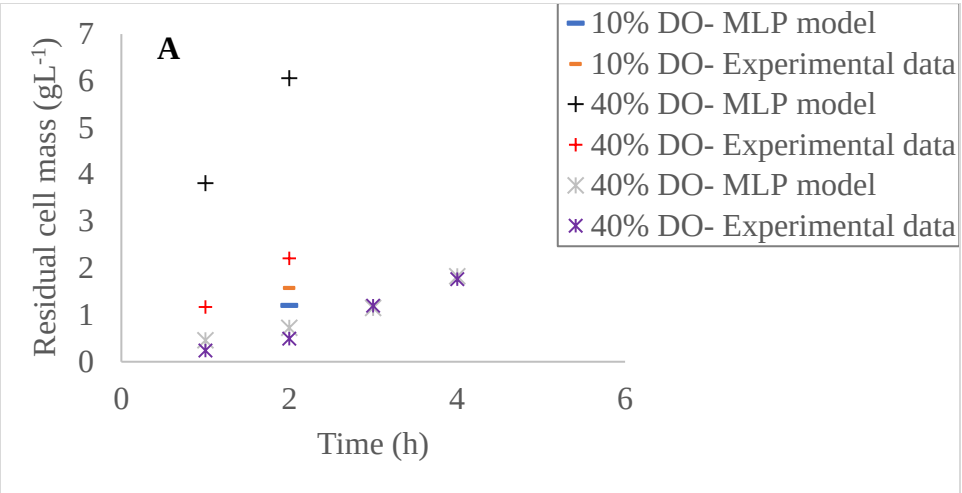

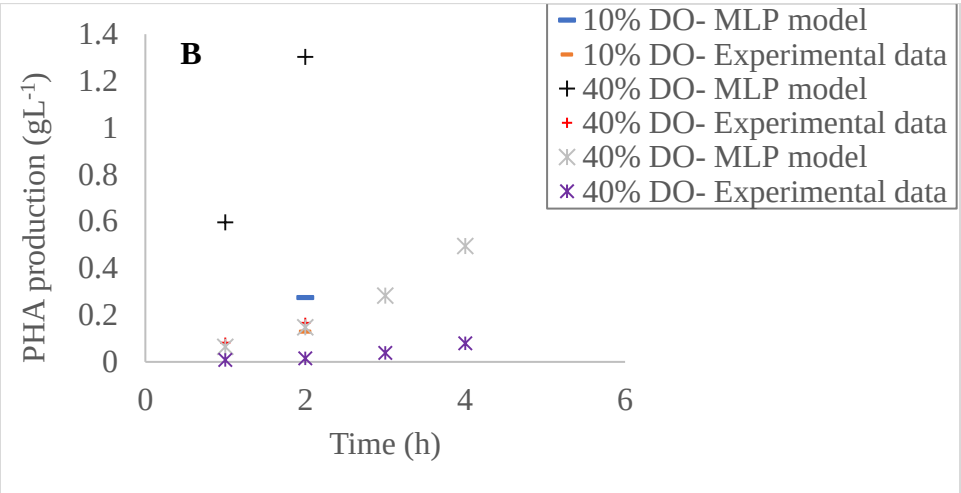

Figure 3-8 Validation of MLP [2,1] under oxygen excess conditions (A) growth, B) PHA production).

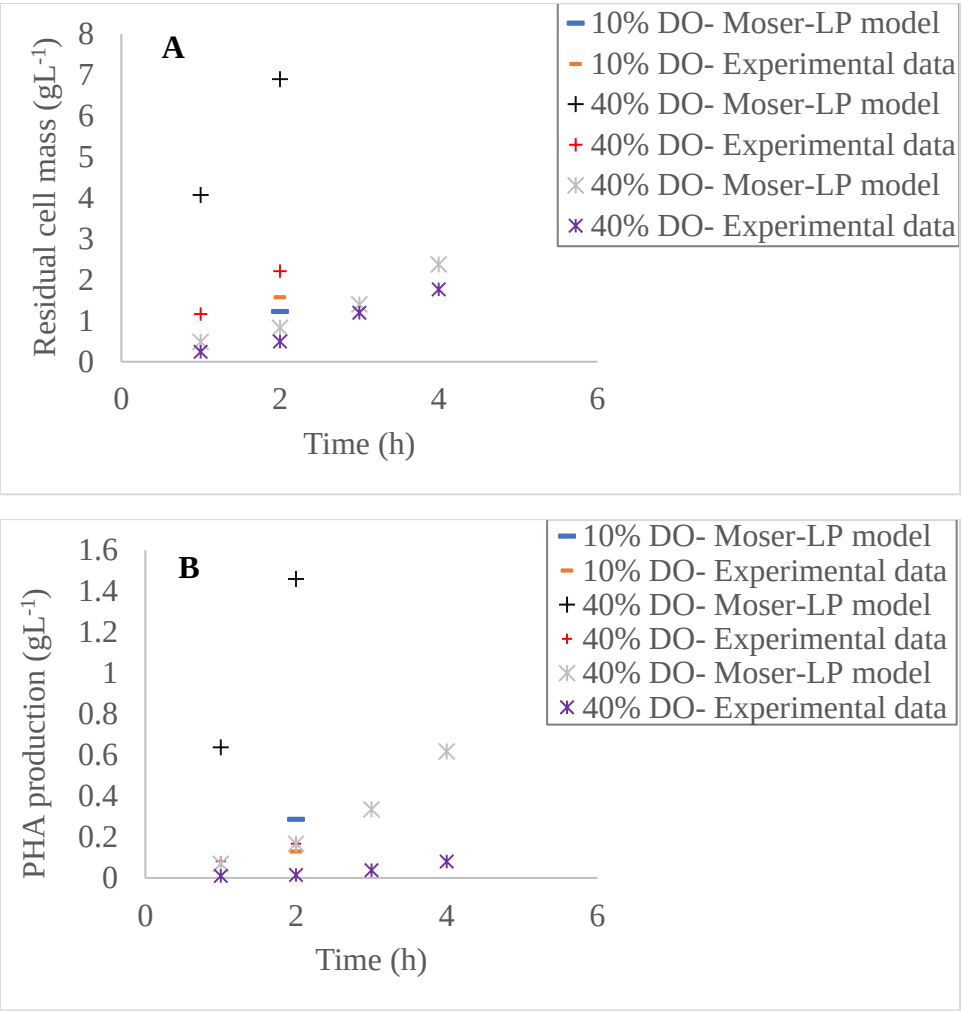

Figure 3-9 Validation of Moser-LP [2,1] under oxygen excess conditions (A) growth, B) PHA production).

Chapter 4

Conclusions, Study Limitations, and Recommendations for Future Work

In order to model the growth and production of mcl-PHAs by *Pseudomonas putida* LS46 cultured with octanoic acid under oxygen-limited conditions in the batch mode residual cell mass, X_r, was used for modeling. The experiments were performed at 0%, 1%, 5%, 10%, and 40% DO. Among the four models, the Monod model with incorporated Leudeking–Piret (MLP), the Moser model with incorporated Leudeking–Piret (Moser-LP), the Logistic model with incorporated Leudeking–Piret (LLP), and the Modified Logistic model with incorporated Leudeking–Piret (MLLP), the MLP and Moser-LP models represented the experimental data closely both for the calibration and validation datasets. These two models had less SAE of calibration and validation (4.174 (MLP), 4.155 (Moser-LP) than the LLP and MLLP models (6.805 and 7.041). In addition, the comparison between the calibrated value of μ_{max} with its experimental value (0.578 ± 0.142) confirmed that MLP and Moser-LP models with calculated maximum growth rate of 0.497 and 0.622 were both reasonably good fits. These two models also indicated that the variables, limiting-substrate concentration (oxygen), initial biomass concentration, initial PHA concentration, and time have effects on growth and PHA production under the experimental conditions. The other models, LLP and MLLP, may work for systems with different experimental conditions. Dhanasekar et al. (2003) showed LLP model could represent the batch kinetics of P(3HB) production by mutant *A. vinelandii* using glucose. Results of this thesis also illustrated that the MLP and Moser-LP models cannot adequately simulate PHA production at 10% and 40% DO, confirming the fact that the models were not valid under oxygen excess conditions. For growth this deviation was not very significant, as growth did not change very considerably under the oxygen-excess conditions.

One of the main limitations of this study was the availability of the experimental data. There were only 25 reliable data points used for model calibration and validation and only 6 reliable data points to investigate the validity of the model under oxygen excess conditions. In order to make more solid conclusions about the validity of the calibrated models, the same methodology used in this thesis should be applied when more data points are collected. Future work could optimize the growth and PHA production by *Pseudomonas putida* LS46 grown on different carbon sources which may reveal patterns that may be useful for enhanced production of PHA polymers. Also, modeling the system in fed-batch and continuous mode could assist in the development of strategies for industrial-scale production.

The engineering significance of the work presented in this thesis is that these models can be applied for modeling the growth and production of mcl-PHAs by *Pseudomonas putida* LS46 cultured with octanoic acid under oxygen-limited conditions in the fed-batch mode. In fed-batch fermentation systems in which nutrients are added to the bioreactors at specific times in the fermentation process, the selected models may be used to predict cell growth and mcl-PHA production in each separate phase of the fed-batch process. If the models are not able to simulate the fed-batch system adequately, the same methodology used in this thesis (calibrating the models with the experimental data) could be applied.

References

Abramowitz, M. 1968. "IA (Ed.) Stegun. Handbook of mathematical functions." In.: Dover Publications, New York.

Achen, C. H. 1982. *Interpreting and using regression* (Sage).

Andrews, J. F. 1968. 'A mathematical model for the continuous culture of microorganisms utilizing inhibitory substrates', *Biotechnology and Bioengineering*, 10: 707-23.

Annuar, M. S. M., I. K. P. Tan, S. Ibrahim, and K. B. Ramachandran. 2008. 'A kinetic model for growth and biosynthesis of medium-chain-length poly-(3-hydroxyalkanoates) in Pseudomonas putida', *Brazilian Journal of Chemical Engineering*, 25: 217-28.

Arthur, C., J. Baker, and H. Bamford. 2008. "International research workshop on the occurrence, effects, and fate of microplastic marine debris." In *Conference Proceedings. Sept*, 9-11.

Asadzadeh, M., and B. Tolson. 2011. 'Hybrid Pareto archived dynamically dimensioned search for multi-objective combinatorial optimization: application to water distribution network design', *Journal of Hydroinformatics*, 14: 192-205.

Asadzadeh, M., and B. Tolson. 2013. 'Pareto archived dynamically dimensioned search with hypervolume-based selection for multi-objective optimization', *Engineering Optimization*, 45: 1489-509.

Asadzadeh, M., and B. A. Tolson. 2009. "A new multi-objective algorithm, Pareto archived DDS." In *Proceedings of the 11th Annual Conference Companion on Genetic and Evolutionary Computation Conference: Late Breaking Papers*, 1963-66. ACM.

Asadzadeh, M., B. A. Tolson, and D. H. Burn. 2014. 'A new selection metric for multiobjective hydrologic model calibration', *Water Resources Research*, 50: 7082-99.

Babel, W., and A. Steinbüchel. 2001. 'Advances in Biochemical Engineering Biotechnology, Volume 071, Biopolyesters'.

Blackman, F. F. 1905. 'Optima and limiting factors', *Annals of Botany*, 19: 281-95.

Blunt, W. 2018. 'The role of low oxygen microenvironments in microbial polyhydroxyalkanoate production using Pseudomonas putida and application to bioreactor operations for improved productivity', University of Manitoba.

Blunt, W., C. Dartiailh, R. Sparling, D. Gapes, D. Levin, and N. Cicek. 2017. 'Microaerophilic environments improve the productivity of medium chain length polyhydroxyalkanoate biosynthesis from fatty acids in Pseudomonas putida LS46', *Process Biochemistry*, 59: 18-25.

Blunt, W., C. Dartiailh, R. Sparling, D. Gapes, D. B. Levin, and N. Cicek. 2018. 'Carbon flux to growth or polyhydroxyalkanoate synthesis under microaerophilic conditions is affected by fatty acid chain-length in Pseudomonas putida LS46', *Applied Microbiology and Biotechnology*, 102: 6437-49.

Budde, C. F., A. E. Mahan, J. Lu, C. Rha, and A. J. Sinskey. 2010. 'Roles of Multiple Acetoacetyl Coenzyme A Reductases in Polyhydroxybutyrate Biosynthesis in Ralstonia eutropha H16', *Journal of Bacteriology*, 192: 5319-28.

Carranza, E. J. M. 2008. *Geochemical anomaly and mineral prospectivity mapping in GIS* (Elsevier).

Chanprateep, S. 2010. 'Current trends in biodegradable polyhydroxyalkanoates', *Journal of Bioscience and Bioengineering*, 110: 621-32.

Chen, G.-Q. 2009. 'A microbial polyhydroxyalkanoates (PHA) based bio-and materials industry', *Chemical Society Reviews*, 38: 2434-46.

Chen, G., G. Zhang, S. Park, and S. Lee. 2001. 'Industrial scale production of poly (3-hydroxybutyrate-co-3-hydroxyhexanoate)', *Applied Microbiology and Biotechnology*, 57: 50-55.

Choi, J.-I., and S. Y. Lee. 1997. 'Process analysis and economic evaluation for poly (3-hydroxybutyrate) production by fermentation', *Bioprocess Engineering*, 17: 335-42.

Choi, J., and S. Y. Lee. 1999. 'Factors affecting the economics of polyhydroxyalkanoate production by bacterial fermentation', *Applied Microbiology and Biotechnology*, 51: 13-21.

Contois, D. 1959. 'Kinetics of bacterial growth: relationship between population density and specific growth rate of continuous cultures', *Microbiology*, 21: 40-50.

De Waard, P., H. Van Der Wal, G. Huijberts, and G. Eggink. 1993. 'Heteronuclear NMR analysis of unsaturated fatty acids in poly (3-hydroxyalkanoates). Study of beta-oxidation in Pseudomonas putida', *Journal of Biological Chemistry*, 268: 315-19.

Deb, K., M. Mohan, and S. Mishra. 2003. 'A fast multi-objective evolutionary algorithm for finding well-spread pareto-optimal solutions (KanGAL Report No. 2003002)', *Kanpur, India: Indian Institute of Technology*.

Dhanasekar, R., T. Viruthagiri, and P. L. Sabarathinam. 2003. 'Poly(3-hydroxy butyrate) synthesis from a mutant strain Azotobacter vinelandii utilizing glucose in a batch reactor', *Biochemical Engineering Journal $V 16*: 1-8.

Dias, J., A. Oehmen, L. Serafim, P. Lemos, M. Reis, and R. Oliveira. 2008. 'Metabolic modelling of polyhydroxyalkanoate copolymers production by mixed microbial cultures', *BMC Systems Biology*, 2: 59.

Digregorio, B. E. 2009. 'Biobased performance bioplastic: Mirel', *Chemistry and Biology*, 16: 1-2.

Dubitzky, W., O. Wolkenhauer, H. Yokota, and K.-H. Cho. 2013. *Encyclopedia of systems biology* (Springer Publishing Company, Incorporated).

Eggink, G., P. De Waard, and G. Huijberts. 1992. 'The role of fatty acid biosynthesis and degradation in the supply of substrates for poly (3-hydroxyalkanoate) formation in Pseudomonas putida', *FEMS Microbiology Reviews*, 9: 159-63.

El Yafrani, M., and B. Ahiod. 2016. "Population-based vs. single-solution heuristics for the travelling thief problem." In *Proceedings of the Genetic and Evolutionary Computation Conference 2016*, 317-24.

Follonier, S., B. Henes, S. Panke, and M. Zinn. 2012. 'Putting cells under pressure: A simple and efficient way to enhance the productivity of medium-chain-length polyhydroxyalkanoate in processes with Pseudomonas putida KT2440', *Biotechnology and Bioengineering*, 109: 451-61.

Gao, J., J. A. Ramsay, and B. A. Ramsay. 2016. 'Fed-batch production of poly-3-hydroxydecanoate from decanoic acid', *Journal of Biotechnology*, 218: 102-07.

Garcia-Ochoa, F., and E. Gomez. 2009. 'Bioreactor scale-up and oxygen transfer rate in microbial processes: an overview', *Biotechnology Advances*, 27: 153-76.

Grousseau, E., E. Blanchet, S. Déléris, M. G. Albuquerque, E. Paul, and J.-L. Uribelarrea. 2013. 'Impact of sustaining a controlled residual growth on polyhydroxybutyrate yield and production kinetics in Cupriavidus necator', *Bioresource Technology*, 148: 30-38.

Hazer, B., and A. Steinbüchel. 2007. 'Increased diversification of polyhydroxyalkanoates by modification reactions for industrial and medical applications', *Applied Microbiology and Biotechnology*, 74: 1-12.

Heinzle, E., and R. Lafferty. 1980. 'A kinetic model for growth and synthesis of poly-β-hydroxybutyric acid (PHB) in Alcaligenes eutrophus H 16', *European Journal of Applied Microbiology and Biotechnology*, 11: 8-16.

Hoffmann, N., and B. H. Rehm. 2004. 'Regulation of polyhydroxyalkanoate biosynthesis in Pseudomonas putida and Pseudomonas aeruginosa', *FEMS Microbiology Letters*, 237: 1-7.

Holmes, P. 1985. 'Applications of PHB-a microbially produced biodegradable thermoplastic', *Physics in Technology*, 16: 32.

Hopewell, J., R. Dvorak, and E. Kosior. 2009. 'Plastics recycling: challenges and opportunities', *Philosophical Transactions of the Royal Society B: Biological Sciences*, 364: 2115-26.

Horvat, P., I. Špoljarić, M. Lopar, A. Atlić, M. Koller, and G. Braunegg. 2013. 'Mathematical modelling and process optimization of a continuous 5-stage bioreactor cascade for production of poly [-(R)-3-hydroxybutyrate] by Cupriavidus necator', *Bioprocess and Biosystems Engineering*, 36: 1235-50.

Huijberts, G., G. Eggink, P. De Waard, G. W. Huisman, and B. Witholt. 1992. 'Pseudomonas putida KT2442 cultivated on glucose accumulates poly (3-hydroxyalkanoates) consisting of saturated and unsaturated monomers', *Applied and Environmental Microbiology*, 58: 536-44.

Iftikhar, A., and N. Jamil. 2016. 'Polyhydroxyalkanoates: current applications in the medical field', *Frontiers in Biology*, 11: 19-27.

Iwata, T. 2015. 'Biodegradable and bio-based polymers: future prospects of eco-friendly plastics', *Angewandte Chemie International Edition in English*, 54: 3210-5.

Jambeck, J. R., R. Geyer, C. Wilcox, T. R. Siegler, M. Perryman, A. Andrady, R. Narayan, and K. L. Law. 2015. 'Plastic waste inputs from land into the ocean', *Science*, 347: 768-71.

Jendrossek, D., and R. Handrick. 2002. 'Microbial degradation of polyhydroxyalkanoates', *Annual Review of Microbiology*, 56: 403-32.

Jiang, Y., M. Hebly, R. Kleerebezem, G. Muyzer, and M. Van Loosdrecht. 2011. 'Metabolic modeling of mixed substrate uptake for polyhydroxyalkanoate (PHA) production', *Water Research*, 45: 1309-21.

Kaur, G., and I. Roy. 2015. 'Strategies for large-scale production of polyhydroxyalkanoates', *Chemical and Biochemical Engineering Quarterly*, 29: 157-72.

Kavunnikova, E., B. Starovoitova, S. Golovin, and A. Krivtsov. 2019. "Comparison of design optimization algorithms of a multiply fractured horizontal well." In *Journal of Physics: Conference Series*, 012029. IOP Publishing.

Keshavarz, T., and I. Roy. 2010. 'Polyhydroxyalkanoates: bioplastics with a green agenda', *Current Opinion in Microbiology*, 13: 321-6.

King, G. 1986. 'How not to lie with statistics: Avoiding common mistakes in quantitative political science', *American Journal of Political Science*: 666-87.

Koch, A. L. 1997. 'Microbial physiology and ecology of slow growth', *Microbiology and Molecular Biology Reviews*, 61: 305-18.

Kollat, J. B., and P. M. Reed. 2005. "The value of online adaptive search: a performance comparison of NSGAII, ε-NSGAII and εMOEA." In *International Conference on Evolutionary Multi-Criterion Optimization*, 386-98. Springer.

Koller, M., P. Horvat, P. Hesse, R. Bona, C. Kutschera, A. Atlić, and G. Braunegg. 2006. 'Assessment of formal and low structured kinetic modeling of polyhydroxyalkanoate synthesis from complex substrates', *Bioprocess and Biosystems Engineering*, 29: 367-77.

Kourmentza, C., J. Placido, N. Venetsaneas, A. Burniol-Figols, C. Varrone, H. N. Gavala, and M. a. M. Reis. 2017. 'Recent Advances and Challenges towards Sustainable Polyhydroxyalkanoate (PHA) Production', *Bioengineering (Basel)*, 4.

Kresic, N. 2006. *Hydrogeology and groundwater modeling* (CRC press).

Kshirsagar, P. R., R. Suttar, S. S. Nilegaonkar, S. Pradhan, and P. P. Kanekar. 2013. 'Scale up production of polyhydroxyalkanoate (PHA) at different aeration, agitation and controlled dissolved oxygen levels in fermenter using Halomonas campisalis MCM B-1027', *Journal of Biochemical Technology*, 4: 512-17.

Lageveen, R. G., G. W. Huisman, H. Preusting, P. Ketelaar, G. Eggink, and B. Witholt. 1988. 'Formation of polyesters by Pseudomonas oleovorans: effect of substrates on formation and composition of poly-(R)-3-hydroxyalkanoates and poly-(R)-3-hydroxyalkenoates', *Applied and Environmental Microbiology*, 54: 2924-32.

Lee, S. Y. 1996a. 'Bacterial polyhydroxyalkanoates', *Biotechnology and Bioengineering*, 49: 1-14.

Lee, S. Y. 1996b. 'Plastic bacteria? Progress and prospects for polyhydroxyalkanoate production in bacteria', *Trends in Biotechnology*, 14: 431-38.

Lopes, M., M. Mota, and I. Belo. 2013. 'Oxygen mass transfer rate in a pressurized lab-scale stirred bioreactor', *Chemical Engineering & Technology*, 36: 1779-84.

Luong, J. H. 1985. 'Kinetics of ethanol inhibition in alcohol fermentation', *Biotechnology and Bioengineering*, 27: 280-5.

Maclean, H., Z. Sun, J. Ramsay, and B. Ramsay. 2008. 'Decaying exponential feeding of nonanoic acid for the production of medium-chain-length poly (3-hydroxyalkanoates) by Pseudomonas putida KT2440', *Canadian Journal of Chemistry*, 86: 564-69.

Madison, L. L., and G. W. Huisman. 1999. 'Metabolic Engineering of Poly(3-Hydroxyalkanoates): From DNA to Plastic', *Microbiology and Molecular Biology Reviews*, 63: 21-53.

Mahanta, D., M. Borah, and P. Saikia. 2014. 'Study on kinetic models for analysing the bacterial growth rate', *American International Journal of Research in Science, Technology, Engineering and Mathematics*, 8: 68-72.

Marketsandmarkets. 2017. ' Polyhydroxyalkanoate (PHA) Market by Type (Monomers, Co-Polymers, Terpolymers), Manufacturing Technology (Bacterial Fermentation, Biosynthesis, Enzymatic Catalysis), Application (Packaging, Bio Medical, Food Services, Agriculture)'.

Marschessault, R., C. Monasterios, F. Morin, and P. Sundararajan. 1990. 'Chiral poly (β-hydroxyalkanoates): an adaptable helix influenced by the alkane side-chain', *International Journal of Biological Macromolecules*, 12: 158-65.

Masood, F., T. Yasin, and A. Hameed. 2015. 'Production and characterization of Tailor-made polyhydroxyalkanoates by Bacillus cereus FC11', *Pakistan Journal of Zoology*, 47.

Misra, S. K., S. P. Valappil, I. Roy, and A. R. Boccaccini. 2006. 'Polyhydroxyalkanoate (PHA)/inorganic phase composites for tissue engineering applications', *Biomacromolecules*, 7: 2249-58.

Monod, J. 1949. 'The growth of bacterial cultures', *Annual Review of Microbiology*, 3: 371-94.

Moser. 1985. ' Kinetics of batch fermentations', *Biotechnology*, 2.

Mozejko-Ciesielska, J., and R. Kiewisz. 2016. 'Bacterial polyhydroxyalkanoates: Still fabulous?', *Microbiological Research*, 192: 271-82.

Mozumder, M., L. Goormachtigh, L. Garcia-Gonzalez, H. De Wever, and E. Volcke. 2014. 'Modeling pure culture heterotrophic production of polyhydroxybutyrate (PHB)', *Bioresource Technology*, 155: 272-80.

Mrwebi, M. 2004. 'Testing Monod: growth rate as a function of glucose concentration in Saccharomyces cerevisiae', Stellenbosch: University of Stellenbosch.

Narodoslawsky, M., K. Shazad, R. Kollmann, and H. Schnitzer. 2015. 'LCA of PHA production–Identifying the ecological potential of bio-plastic', *Chemical and Biochemical Engineering Quarterly*, 29: 299-305.

Neeleman, R. 2002. *Biomass performance: monitoring and control in bio-pharmaceutical production*.

Ningthoujam, S. S., A. D. Talukdar, S. D. Sarker, L. Nahar, and M. D. Choudhury. 2018. 'Prediction of Medicinal Properties Using Mathematical Models and Computation, and Selection of Plant Materials.' in, *Computational Phytochemistry* (Elsevier).

Novak, M., M. Koller, G. Braunegg, and P. Horvat. 2015. 'Mathematical Modelling as a Tool for Optimized PHA Production', *Chemical and Biochemical Engineering Quarterly*, 29: 183-220.

Okpokwasili, G., and C. Nweke. 2006. 'Microbial growth and substrate utilization kinetics', *African Journal of Biotechnology*, 5: 305-17.

Plasticseurope. 2012. 'Plastics—the Facts 2012. An Analysis of European Plastics Production, Demand and Waste Data for 2011'.

Plasticseurope. 2016. ' Plastics—The Facts 2016. An Analysis of European Plastics Production, Demand and Waste Data'.

Pratt, S., A. Werker, F. Morgan-Sagastume, and P. Lant. 2012. 'Microaerophilic conditions support elevated mixed culture polyhydroxyalkanoate (PHA) yields, but result in decreased PHA production rates', *Water Science and Technology*, 65: 243-6.

Prieto, A., I. F. Escapa, V. Martínez, N. Dinjaski, C. Herencias, F. De La Peña, N. Tarazona, and O. Revelles. 2016. 'A holistic view of polyhydroxyalkanoate metabolism in Pseudomonas putida', *Environmental Microbiology*, 18: 341-57.

Raghuvanshi, S., and B. Babu. 2010. 'Biodegradation kinetics of methyl iso-butyl ketone by acclimated mixed culture', *Biodegradation*, 21: 31.

Raje, P., and A. Srivastava. 1998. 'Updated mathematical model and fed-batch strategies for poly-β-Hydroxybutyrate (PHB) production by Alcaligenes eutrophus', *Bioresource Technology*, 64: 185-92.

Rardin, R. L., and R. Uzsoy. 2001. 'Experimental evaluation of heuristic optimization algorithms: A tutorial', *Journal of Heuristics*, 7: 261-304.

Rochman, C. M., M. A. Browne, B. S. Halpern, B. T. Hentschel, E. Hoh, H. K. Karapanagioti, L. M. Rios-Mendoza, H. Takada, S. Teh, and R. C. Thompson. 2013. 'Policy: Classify plastic waste as hazardous', *Nature*, 494: 169.

Rodriguez-Perez, S., A. Serrano, A. Pantión, and B. Alonso-Fariñas. 2018. 'Challenges of scaling-up PHA production from waste streams. A review', *Journal of environmental management*, 205: 215-30.

Sahraei, S., M. Asadzadeh, and M. Shafii. 2019. 'Toward effective many-objective optimization: Rounded-archiving', *Environmental Modelling & Software*, 122: 104535.

Schmidt, M., J. L. Ienczak, L. K. Quines, K. Zanfonato, W. Schmidell, and G. M. F. De Aragão. 2016. 'Poly (3-hydroxybutyrate-co-3-hydroxyvalerate) production in a system with external cell recycle and limited nitrogen feeding during the production phase', *Biochemical Engineering Journal*, 112: 130-35.

Senior, P., G. Beech, G. Ritchie, and E. Dawes. 1972. 'The role of oxygen limitation in the formation of poly-β-hydroxybutyrate during batch and continuous culture of Azotobacter beijerinckii', *Biochemical Journal*, 128: 1193-201.

Sin, G., D. J. De Pauw, S. Weijers, and P. A. Vanrolleghem. 2008. 'An efficient approach to automate the manual trial and error calibration of activated sludge models', *Biotechnology and Bioengineering*, 100: 516-28.

Somleva, M. N., K. D. Snell, J. J. Beaulieu, O. P. Peoples, B. R. Garrison, and N. A. Patterson. 2008. 'Production of polyhydroxybutyrate in switchgrass, a value-added co-product in an important lignocellulosic biomass crop', *Plant Biotechnology Journal*, 6: 663-78.

Sudesh, K., H. Abe, and Y. Doi. 2000. 'Synthesis, structure and properties of polyhydroxyalkanoates: biological polyesters', *Progress in Polymer Science*, 25: 1503-55.

Talbi, E.-G. 2009. *Metaheuristics: from design to implementation* (John Wiley & Sons).

Thompson, R. C., Y. Olsen, R. P. Mitchell, A. Davis, S. J. Rowland, A. W. John, D. Mcgonigle, and A. E. Russell. 2004. 'Lost at sea: where is all the plastic?', *Science*, 304: 838-38.

Thompson, R. C., S. H. Swan, C. J. Moore, and F. S. Vom Saal. 2009. 'Our plastic age', *Philosophical Transactions of the Royal Society B*, 364: 1973-6.

Tohyama, M., T. Patarinska, Z. Qiang, and K. Shimizu. 2002. 'Modeling of the mixed culture and periodic control for PHB production', *Biochemical Engineering Journal*, 10: 157-73.

Tolson, B. A., and C. A. Shoemaker. 2007. 'Dynamically dimensioned search algorithm for computationally efficient watershed model calibration', *Water Resources Research*, 43.

Trucano, T. G., L. P. Swiler, T. Igusa, W. L. Oberkampf, and M. Pilch. 2006. 'Calibration, validation, and sensitivity analysis: What's what', *Reliability Engineering & System Safety*, 91: 1331-57.

Van Hentenryck, P., L. Michel, and Y. Deville. 1997. *Numerica: a modeling language for global optimization* (MIT press).

Vidhya, C., and R. Aasha. 2018. 'Isolation, optimization and production of polyhydroxyalkanoates (PHA) from soil bacteria'.

Williams, S. F., D. P. Martin, D. M. Horowitz, and O. P. Peoples. 1999. 'PHA applications: addressing the price performance issue: I. Tissue engineering', *International Journal of Biological Macromolecules*, 25: 111-21.

Worm, B., H. K. Lotze, I. Jubinville, C. Wilcox, and J. Jambeck. 2017. 'Plastic as a Persistent Marine Pollutant', *Annual Review of Environment and Resources*, 42: 1-26.

Yu, J., Y. Si, W. Keung, and R. Wong. 2002. 'Kinetics modeling of inhibition and utilization of mixed volatile fatty acids in the formation of polyhydroxyalkanoates by Ralstonia eutropha', *Process Biochemistry*, 37: 731-38.

Zinn, M., B. Witholt, and T. Egli. 2001. 'Occurrence, synthesis and medical application of bacterial polyhydroxyalkanoate', *Advanced Drug Delivery Reviews*, 53: 5-21.

Appendix A

Figure A1 to Figure A8 show the dissolved oxygen concentrations, octanoic concentrations, cell growth, and PHA production curves for one 0% DO data set (Figure A1), for 1% (Figure A2 and Figure A3) and 5% (Figure A4 and Figure A5) DO, for one 10% (Figure A6) DO data set, and for two 40% (Figure A7 and Figure A8) DO data sets (Table 2.1). For 0% DO, data from 6 to 11 h was used for modeling, and the 6 h time point was considered as time zero in modeling this data set, because before 6 h, the dissolved oxygen concentration was not constant, and after 11 h the system was under carbon-limited conditions instead of oxygen-limited conditions (Figure A1). The same rationale was applied to the 6 -12 h and 7-10 h time points for the two 1% DO data sets (Figure A2 and Figure A3), the 6-9 h and 7-10 h time points for the 5% DO data sets (Figure A4 and Figure A5), the 6-8 h time points for the 10% D) (Figure A6), and the 6-8 and 4-8 h time points for the 40% DO (Figure A7 and Figure A8) data sets.

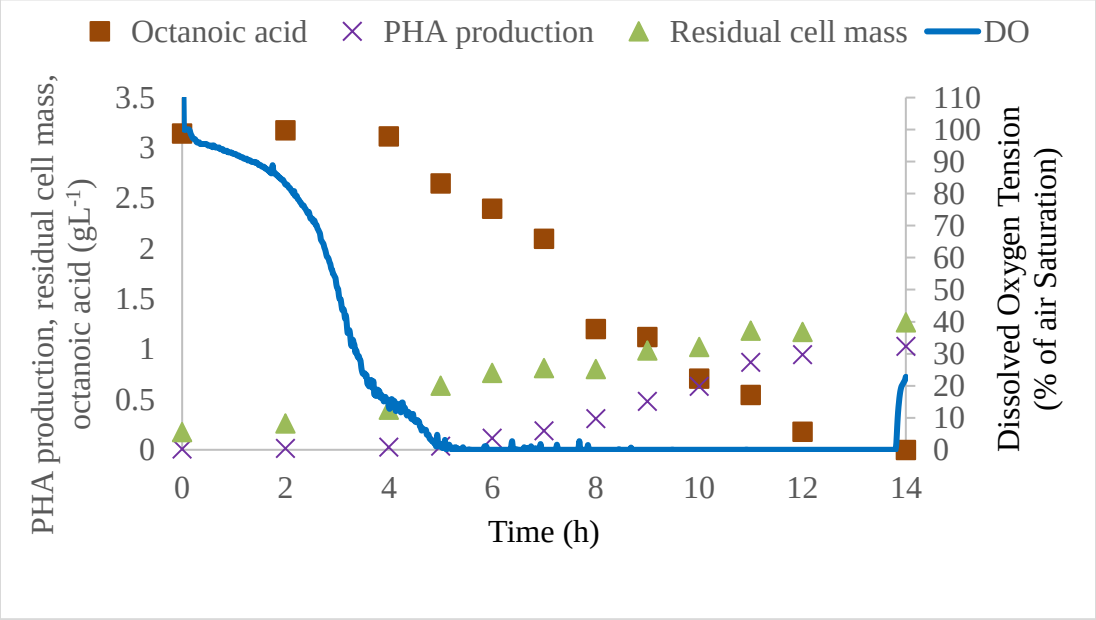

Figure A1 Representative DO, growth and PHA production curves from octanoic acid at 0% DO (data set 2) (Adapted from Blunt (2018)).

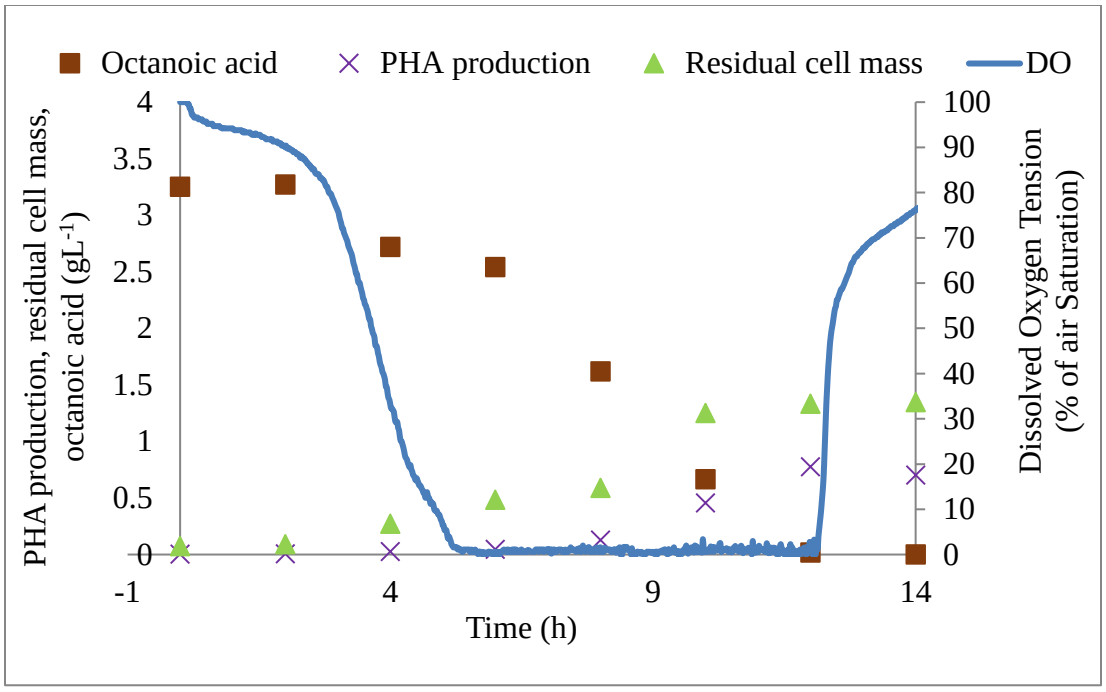

Figure A2 Representative DO, growth and PHA production curves from octanoic acid at 1% DO (data set 1) ((Blunt 2018) data not shown).

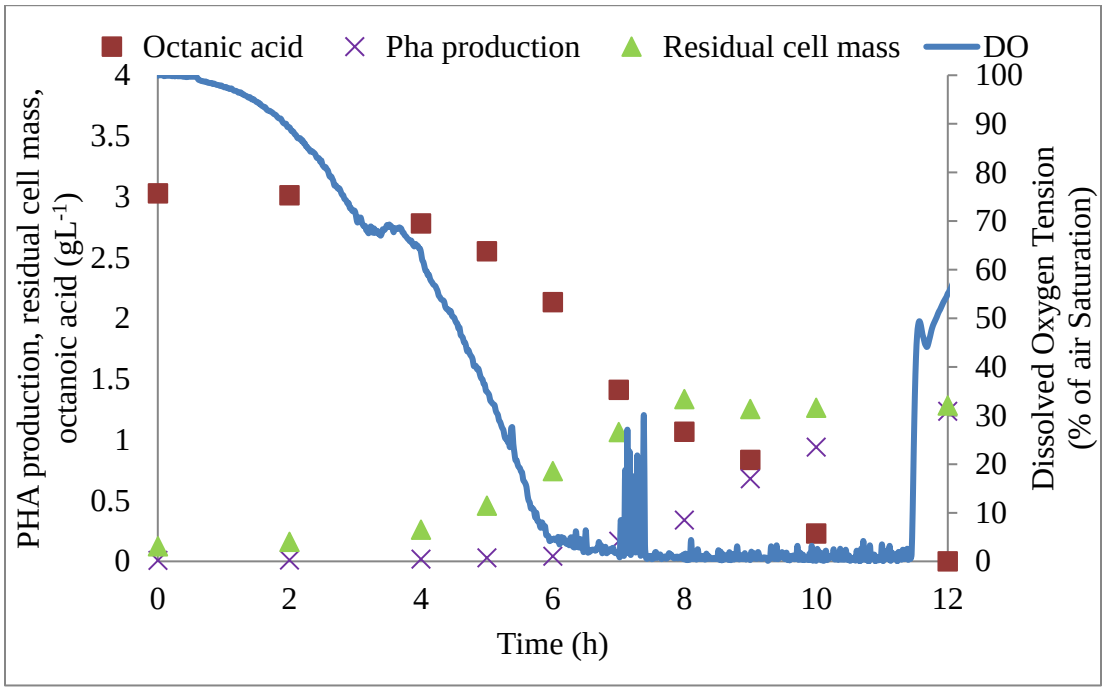

Figure A3 Representative DO, growth and PHA production curves from octanoic acid at 1% DO (data set 2) ((Blunt 2018) data not shown).

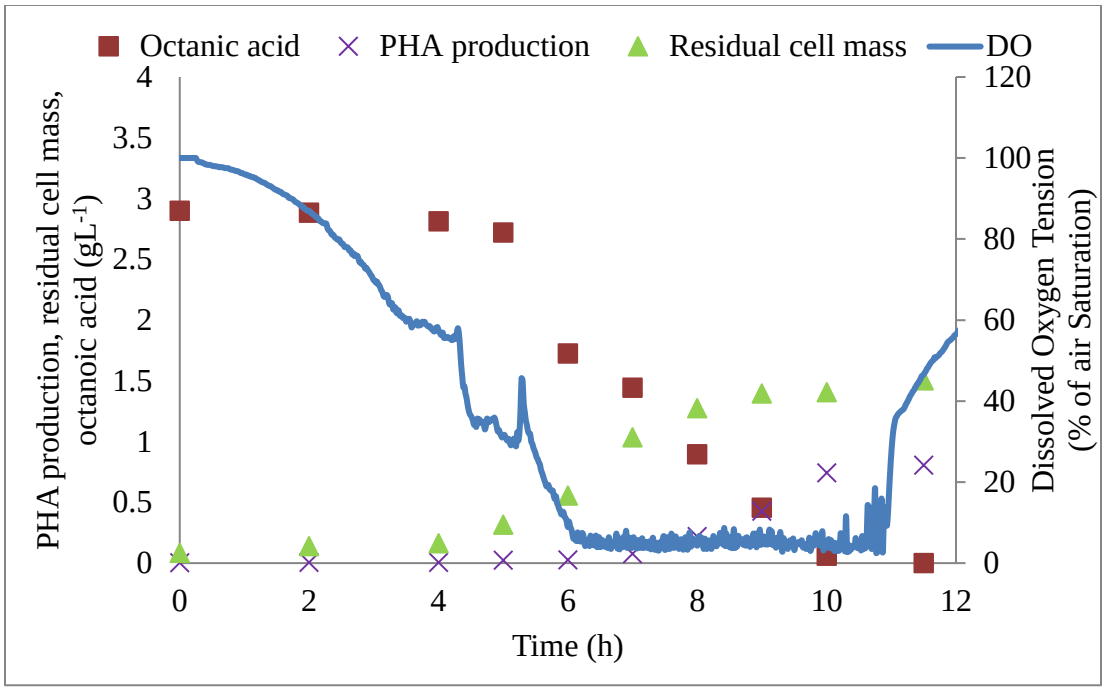

Figure A4 Representative DO, growth and PHA production curves from octanoic acid at 5% DO (data set 1) ((Blunt 2018) data not shown).

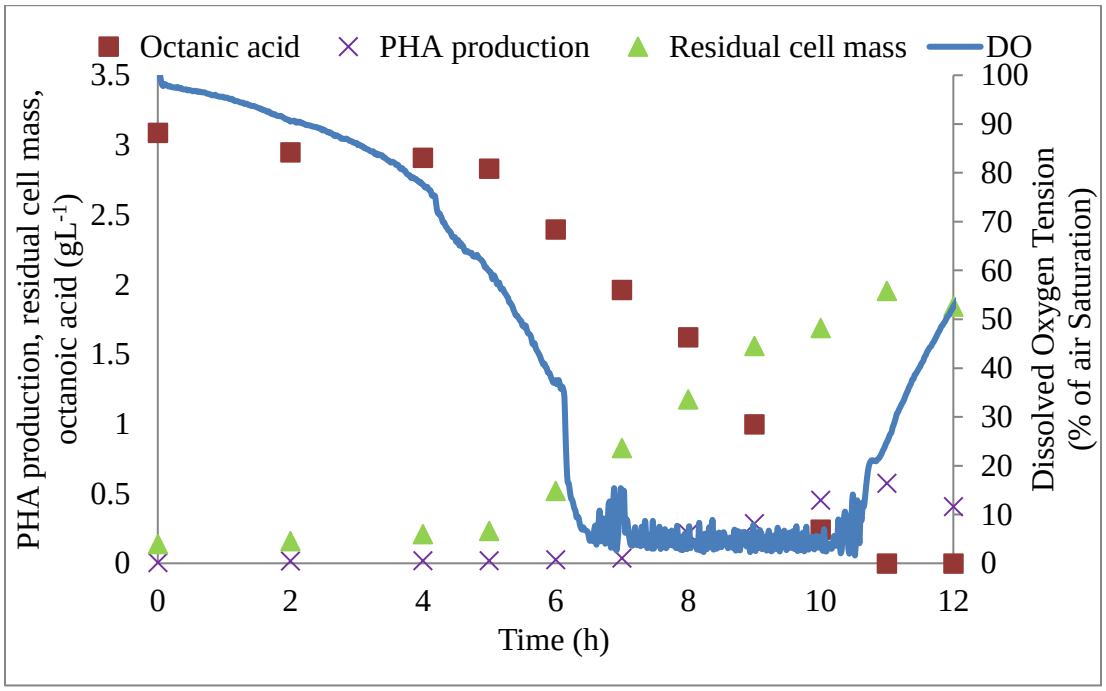

Figure A5 Representative DO, growth and PHA production curves from octanoic acid at 5% DO (data set 2) ((Blunt 2018) data not shown).

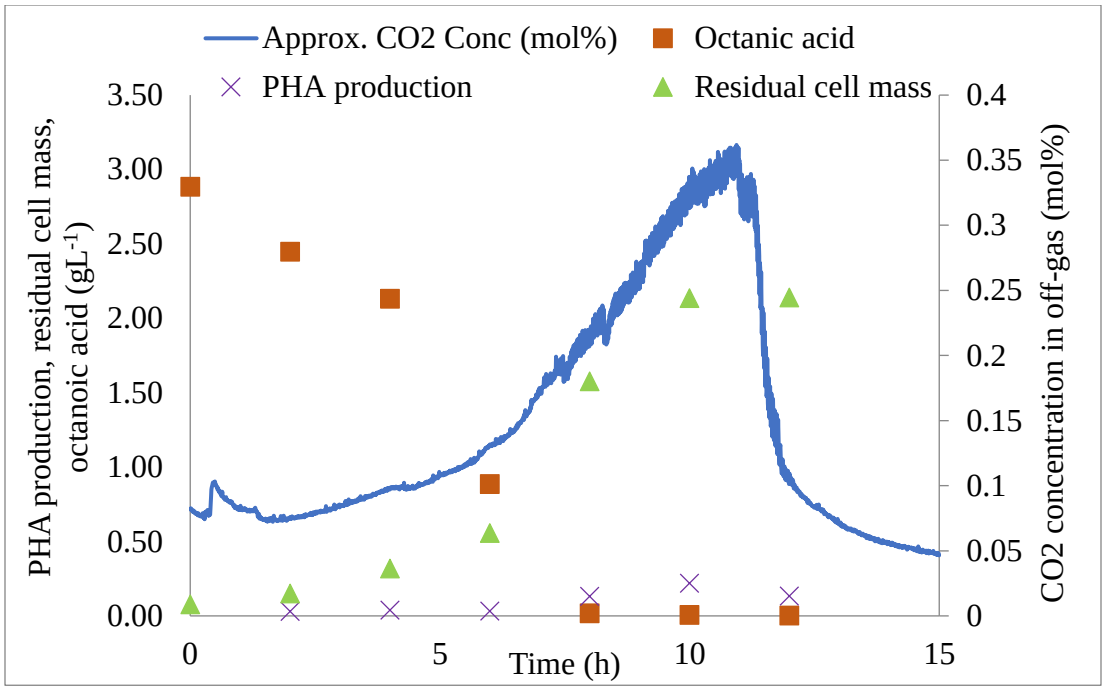

Figure A6 Representative DO, growth and PHA production curves from octanoic acid at 10% DO (data set 1) ((Blunt 2018) data not shown).

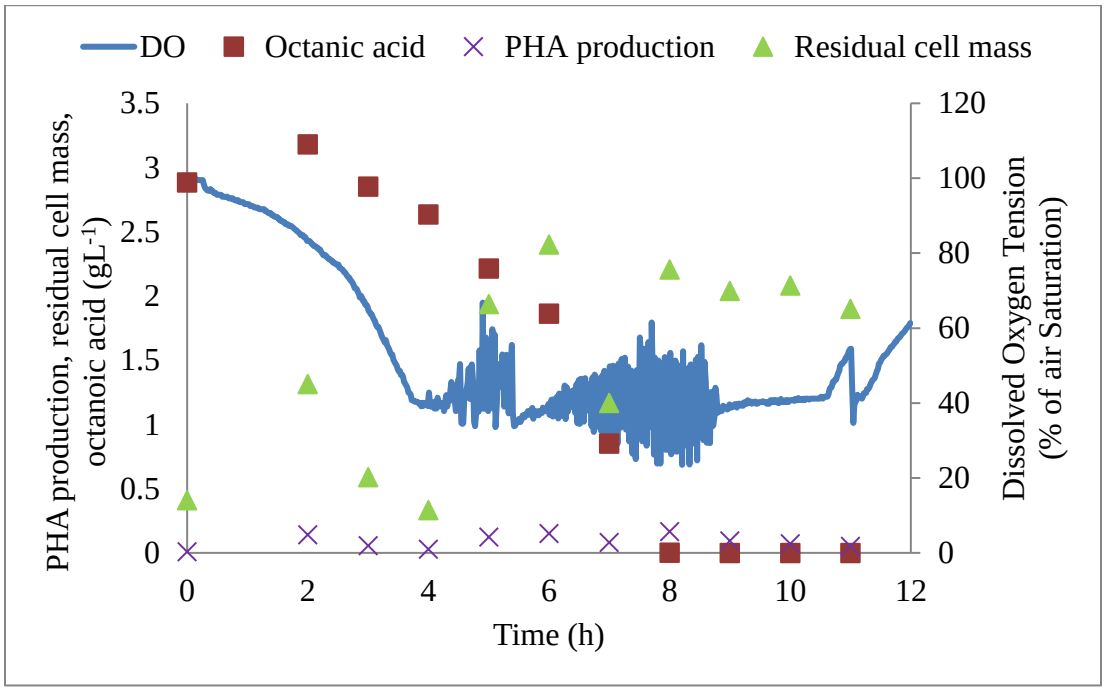

Figure A7 Representative DO, growth and PHA production curves from octanoic acid at 40% DO (data set 1) (Adapted from Blunt (2018)).

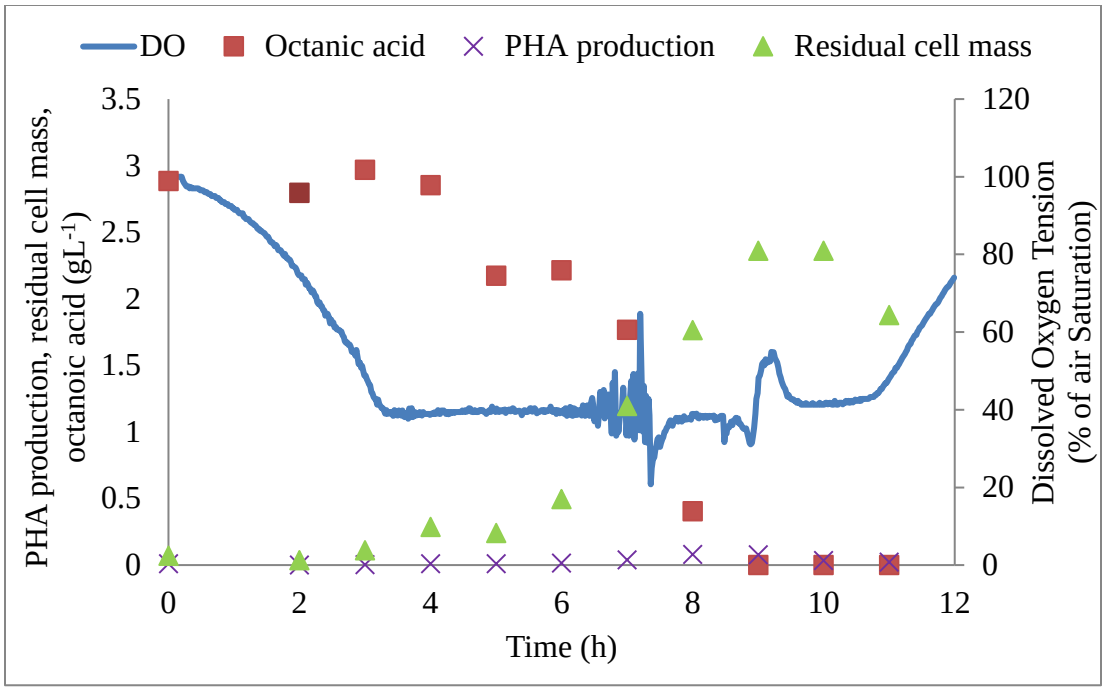

Figure A8 Representative DO, growth and PHA production curves from octanoic acid at 40% DO (data set 2) (Adapted from Blunt (2018)).